doi:10.20944/preprints202110.0008.v1

Article

Low Calcium Cave Dripwaters in a High CO_2 Environment: Formation and Development of Corrosion Cups in Postojna Cave, Slovenia

Lovel Kukuljan[1], Franci Gabrovšek[1,]* and Vanessa E. Johnston[1]

[1] Karst Research Institute ZRC SAZU, Titov trg 2, 6230 Postojna, Slovenia; lovel.kukuljan@zrc-sazu.si, gabrovsek@zrc-sazu.si, vanessa.johnston@zrc-sazu.si
* Correspondence: gabrovsek@zrc-sazu.si; Tel.: +386 5 700 19 07

Abstract: Speleothems have proven to be one of the most reliable terrestrial archives for palaeoclimate research. However, due to the complexity of karst systems, long-term monitoring and high-resolution analyses of the cave atmosphere and water geochemistry have become essential to better constrain the factors that control calcite growth and how geochemical palaeoclimate proxies are encoded into speleothems. While calcite precipitation incorporates the palaeoclimate signals into the speleothem fabric, certain conditions in caves can favour dissolution, which may form hiatuses or even destroy these signals. In extreme cases, in-cave dissolution by dripwater can form cup-shaped features (i.e., corrosion cups), which were the main focus of this study. The study site in Postojna Cave, Slovenia, was investigated through cave climate monitoring and drip and cup water sampling, which took place during 2017–2021. We found that the cups are fed by low calcium drips as the consequence of the thin vadose zone above the cave. Due to the specific configuration of airflow pathways, the study site accumulates high levels of CO_2 (>10,000 ppm), which shifts low calcium dripwater into undersaturation. This causes dissolution on rock surfaces and speleothems on the cave floor. The results of this study have broader significance in addressing the suitability of cave environments and speleothems used in paleoclimate research.

Keywords: speleothem corrosion, undersaturated drip spots, carbon dioxide, cave microclimate, karst water geochemistry

1. Introduction

Speleothems provide robust palaeoclimate archives in continental settings since they can be absolutely dated using U-series methods and contain multiple palaeoclimate proxy records. Although understanding the mechanism of palaeoclimate signal occlusion in stalagmites has been extensively studied, it remains a challenging task due to the inherent complexity of karst systems and the processes involved [1]. Therefore, it is important to fill the knowledge gaps in a broader context: the weather and climate controls, the (bio)geochemistry in the soil zone, the hydrology of the karst vadose zone, the physical and chemical processes on a micro-scale, and finally the conditions in the cave environment that form an incubator for speleothem growth [2–7].

CO_2 is one of the main regulators of speleothem growth because it determines the amount of calcium dissolved in water and the amount precipitated in caves in the form of speleothems. Since CO_2 sources and sinks are highly variable both spatially and temporally, it is important to record the CO_2 distribution in caves and monitor its variations with high resolution [3,8–16]. In mid-latitude, high-latitude and continental caves, seasonal variations in CO_2 partial pressure (pCO_2) are a common feature of the cave climate [3,12,17–19]. The seasonal variations of pCO_2 in cave air and the corresponding variations in calcite deposition rate are usually influenced by cave ventilation, which in turn is frequently driven by the chimney effect [19]. In a typical situation of caves with only one entrance—which can still be ventilated by the chimney effect—more ventilation in one season leads to a reduction of $p\mathrm{CO}_2$ in the cave air, more degassing of the dripwater and more abundant precipitation of calcite [12,19]. In the other season, ventilation may be restricted, for example, in descending caves with only one entrance, which act as cold traps in the warm season and are only ventilated in the colder season when cold and dense outside air flows into the cave [11,12,18]. In such cases, a build-up of CO_2 can limit or prevent calcite precipitation altogether and, in extreme cases, lead to dissolution. Alternatively, lack of or reduced speleothem growth can be associated with colder climates and/or higher altitudes due to a thin soil zone that does not provide sufficient CO_2 for the initial dissolution of the host rock [20].

The growth, architecture and micropetrography of speleothems affected by occasional periods of dissolution have been investigated in only a handful of studies [2,21]. Other studies refer to "hindered stalagmite growth", "near-zero growth" or explicitly of "dissolution by undersaturated dripwater" in certain cave settings but have yet to be subjected to detailed study [14,16,22,23]. However, dissolution in the context of specific processes, such as condensation corrosion [24], mixing corrosion [25], microbially-mediated dissolution [26], hypogene speleogenesis [27] or prior calcite precipitation (PCP) [28], has received some attention. One aim of this work is to investigate the geochemical and cave climate conditions that promote local dissolution in cave rich in speleothems, that results in extensive damage to the speleothems and the palaeoclimate signals that they contain.

A model of the evolution of water-carbonate chemistry in the karst system facilitates understanding of the processes and constraints at a conceptual level [1,29,30]. Due to the rapid kinetics of calcite dissolution, water percolating through the vadose zone reaches equilibrium with calcite and the $p\mathrm{CO}_2$ value of the vadose zone within a few tens of meters. When this water enters a cave where the atmosphere has lower $p\mathrm{CO}_2$ than before, this causes degassing of excess CO_2, leading to supersaturation of the water with respect to calcite and finally calcite precipitation [31]. In a conceptual model of water evolution in Figure 1, these processes are shown with blue arrows. The amount of dissolved calcium depends on the initial $p\mathrm{CO}_2$ in the water and the conditions in the vadose zone, which either replenish CO_2 during dissolution (open system conditions; A to C) or deplete CO_2 (closed system conditions; A to B). Finally, the degree of calcite supersaturation depends on the $p\mathrm{CO}_2$ of the cave air.

At the other end of the extreme, there are several possible scenarios for dissolution in the caves environment, represented by the red arrows in Figure 1:

1. the water arrives in the cave undersaturated (e.g., due to rapid flow and incomplete saturation; E to F) and causes dissolution in the cave (F to G),
2. the water arrives saturated in the cave but encounters a higher $p\mathrm{CO}_2$ than in the vadose zone or it has been saturated under closed system conditions, replenishing the spent CO_2 from the cave air (E to G to H),
3. the dripping water degasses and equilibrates to the low $p\mathrm{CO}_2$ of the cave air, but after a conceivable increase in $p\mathrm{CO}_2$ it equilibrates to this new state (C to D to H),
4. Mixing corrosion due to the effect of undersaturation of the calcite, even if the mixed solutions were previously saturated (not shown).

The strongest dissolution would occur with the greatest $p\mathrm{CO}_2$ fluctuations in the cave air (C to D to H). Weaker precipitation would keep the water well in the supersaturated state, and only a sharp increase in $p\mathrm{CO}_2$ would move the water into the undersaturated region. However, how well such a simple model reflects real-world scenarios depends on the study sites or the observed drip spots, but nevertheless valuable insights can be gained and boundary conditions found.

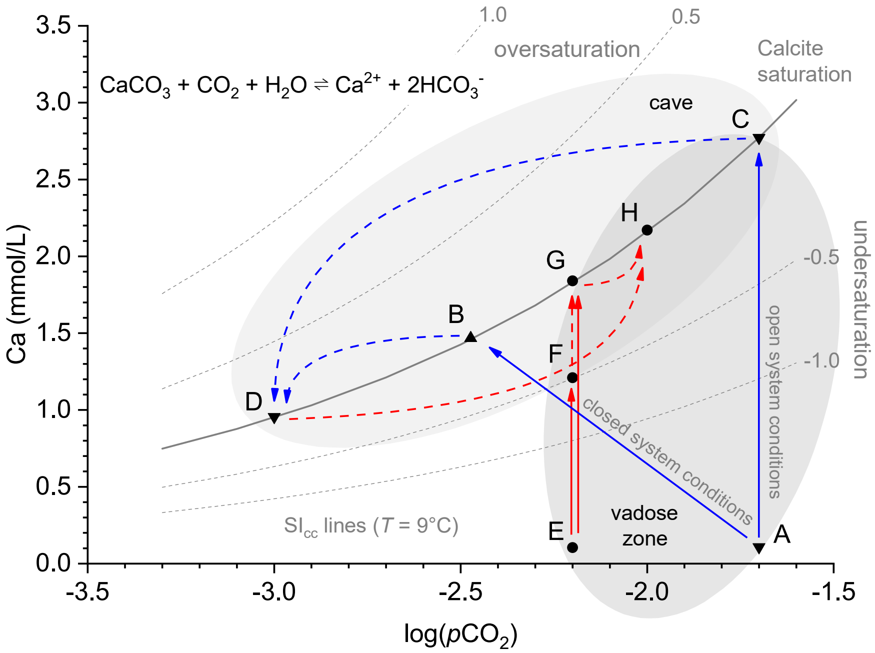

Figure 1. A simplified conceptual model of chemical water evolution in the karst system, showing the dominant processes of solution gassing or degassing and calcite dissolution or precipitation. The solid lines show the processes taking place in the vadose zone, while the dashed lines represent the processes in a cave. Pathways that result in calcite precipitation are shown in blue, while those that cause dissolution are red. The regions with expected Ca concentrations and $\log(p\mathrm{CO_2})$ values for the soil or cave water are shown by grey ellipses. However, the exact position of a particular solution within the pathway is arbitrary, but roughly corresponds to the conditions found in this study. The grey lines with constant saturation indices are calculated for 9 °C. The precipitation pathways (solid blue lines) start from a high CO_2 environment at point A ($p\mathrm{CO_2} = 10^{-1.7}$, ~20,000 ppm). Dissolution of the host rock can follow either a closed system A to B or an open system A to C to reach calcite saturation. Dripwater B or C enters the cave, degasses causing supersaturation with respect to calcite and calcite precipitates towards D (blue dashed lines), which is in equilibrium with the current $p\mathrm{CO_2}$ of the cave air. The dissolution pathways (solid red lines) show water entering the cave either undersaturated with respect to calcite due to incomplete dissolution of the host rock (E to F) allowing calcite dissolution in the cave (F to G) or saturated with calcite that then absorbs CO_2 from the cave air (D to H or G to H) permitting dissolution of cave carbonates.

The aim of this paper is to present an example of calcite dissolution occurring within a cave, thus far presented only theoretically, to investigate the real-world conditions necessary for its occurrence. We examined cup-shaped dissolution features, so-called “corrosion cups”, found in large numbers in the Pisani Passage of Postojna Cave, using cave climate and dripwater monitoring data collected in 2017–2021. Previous studies have found that the Pisani Passage has the highest CO_2 concentrations in Postojna Cave and extreme $p\mathrm{CO_2}$ gradients during warm periods [15,32,33]. In the current study, we compare observations of the cave climate with hydrochemical analyses and use basic models of carbonate chemistry to explain the formation and growth of corrosion cups that has implications for the corrosion of speleothems.

2. Materials and Methods

2.1. Study Site

2.1.1. Postojna Cave

Postojna Cave is a world-famous show cave in central Slovenia near the town of Postojna (Figure 2a). It is an extensive cave system comprising 24 km of passages connected to the surface by five main entrances [34]. The system extends horizontally over several levels—the lower level is epiphreatic and drains the Pivka River, while the upper level is dry and consists of large breakdown chambers and passages decorated with speleothems. The main entrance of the cave is located at the southern end near the Pivka Ponor at 529 m a.s.l. The rock overburden is 30–100 m thick [35]. The cave is located within the extensive Dinaric (NW–SE) fault zones and active micro-deformations are present throughout the cave, especially in breakdown chambers [36]. The cave system is characterised by efficient cave ventilation, which changes direction seasonally. In the colder seasons, an upward airflow (updraft) is observed, directing air from the main entrance of the cave to the higher elevation entrances, while in the warmer seasons, the direction of the airflow is reversed (downdraft). The average ambient cave air temperature is 9–11 °C, depending on the location. The nearest national meteorological station is in Postojna, 1.2 km SSW of the main cave entrance [37]. The average air temperature in Postojna is 9.3 °C, with July being the warmest month (19 °C) and January the coldest (0.1 °C). Postojna receives an average of 1500 mm of precipitation per year, with the least in January, February and July, and the most in September, November and December.

2.1.2. Pisani Passage and Red Hall

Postojna Cave has a few dead-end side-passages, the largest being the Pisani Passage (Figure 2b). The Pisani Passage (PP) is located in the easternmost part of the system and extends ~500 m northwards along the southwest-facing fault zones. The passage is formed in relatively pure Upper Cretaceous limestones, with rare intercalations of chert lenses and dolomitised limestones [38]. The passage is about 5 m wide and 4 m high. The largest spaces associated with the crossing of several active faults [38,39] are in breakdown chambers halfway down the passage (SC Hall) and at the end of the passage (Red Hall, "Rdeča dvorana", abbr. RD, and White Hall, abbr. WH). There, the thickness of the overburden is lowest (~30 m). Apart from breakdown chambers filled with loose rock, the interior of the passage is filled with fluvial sediments remaining from the former river flow and overlain by a rich cover of speleothems. Although there is no accessible opening to the surface, the PP is well ventilated throughout its extent. The average air temperature is 8.8 °C and shows very little seasonal variation (±0.1 °C), but a gradual warming has been observed in recent years [15]. The air $p\mathrm{CO_2}$ dynamics and specific phenomena relevant to this study were investigated previously [15]. The surface above the PP is covered by beech and fir forests with thick rocky soils [40].

The distinct dissolution features in the PP are found in abundance in only two sites already mentioned in earlier studies [38,41]. The first location is in the SC Hall below the high chimney and the other in the lowest section of the Red Hall (Figure 2b and c). The Red Hall and White Hall form a single chamber with a volume of about 6800 m^3. The intersection of prominent faults resulted in the dislodgment and accumulation of boulders covering most of the floor of the passage. The sides and the most distant section are covered with fluvial loam sediments. Many massive (>2 m high and >20 cm diameter) stalagmites have grown over Red and White Hall. In general, all other surfaces are covered by either a thick flowstone cover or a thin flowstone crust of brown or red colour, hence the name Red Hall (Figure 3a). No signs of dissolution features were found on the ceiling of the Red Hall. Soda-straw stalactites predominate on the NE part of the ceiling, while the SW part is mostly bare, indicating relatively recent collapses.

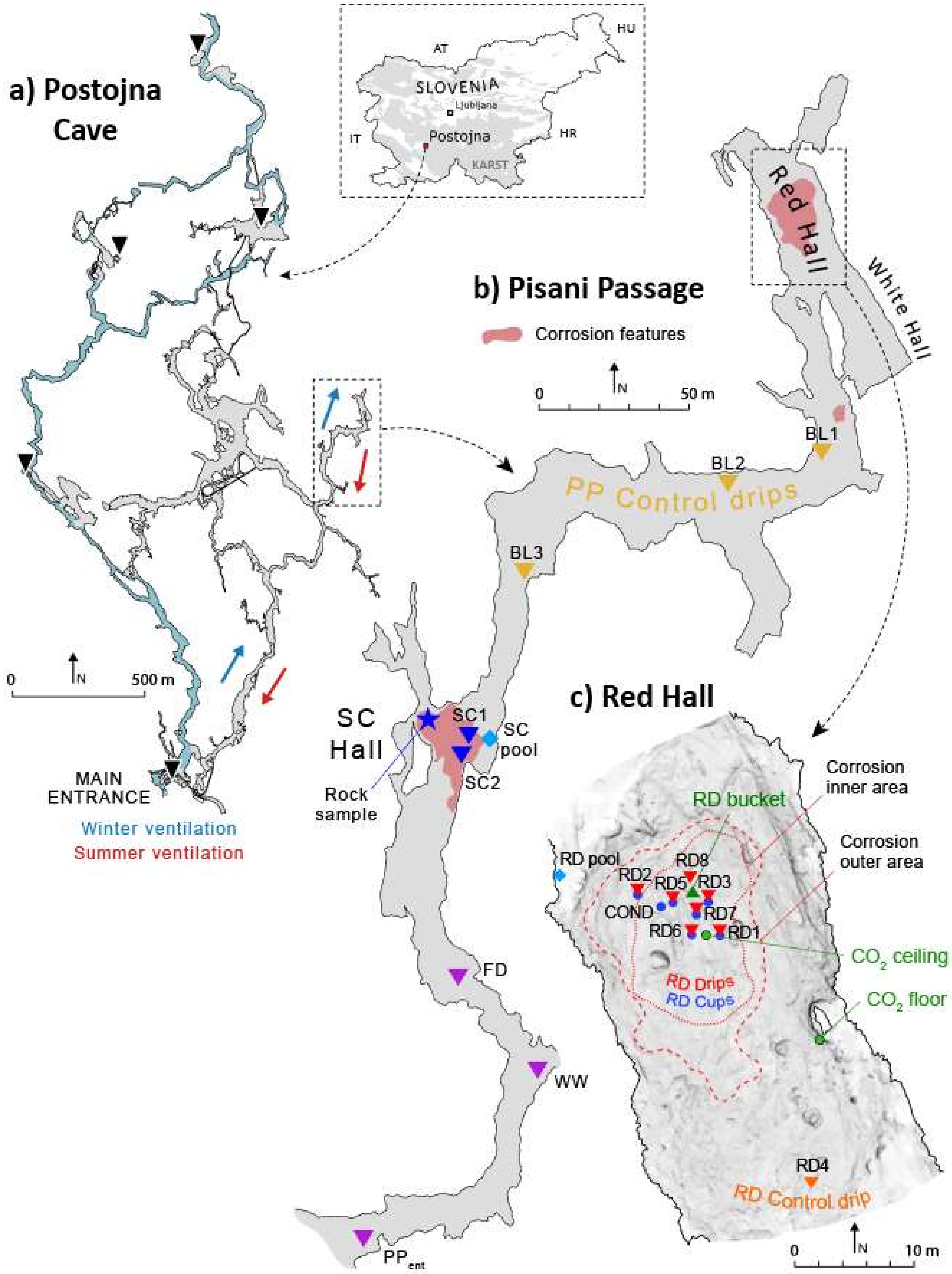

Figure 2. Location of the study site. (**a**) Map of Slovenia showing the location of the cave and plan of Postojna Cave. The typical ventilation pattern is indicated by red and blue arrows showing summer and winter ventilation, respectively; (**b**) Plan of Pisani Passage showing the locations of the numerous corrosion features and sampling sites in Pisani Passage; (**c**) Plan of the Red Hall showing the largest number of corrosion cups in the Pisani Passage. The extent of the corrosion features is indicated by dashed red lines, which are explained in the text. The sampled drip sites are marked with inverted triangles (drips), circles (cups), diamonds (pools) and triangles (bucket). Continuous pCO_2 monitoring sites are indicated by green circles. Map source: Cave cadastre of the Karst Research Institute ZRC SAZU.

Dissolution features are concentrated under active drip spots and exhibit a variety of shapes and sizes, ranging from shallow white indentations where only flowstone crust is dissolved to ~50 cm deep and narrow tubes (Figure 3a). The most common are so-called corrosion cups, which are typically about 5 cm wide and 5–10 cm deep (e.g., RD5 and RD6; Figure 3b), while RD1 is a wide shallow dish shaped feature. Almost 400 corroded drip spots were found only in the localised deepest area in Red Hall. Some drip spots do not form cup-shaped cavities, but rather semi-circular tubes or flutes, especially on sloping surfaces or in cases when the water drains efficiently (Figure 3b). When the dripping water splashes into the cups, some of the water is displaced from the cup and the cups are usually never completely filled with water. The splashing contributes to corrosion of the surfaces surrounding the cup, as can be seen for high-discharge drip RD1 (Figure 3b). The dissolution occurs irrespective of the surfaces, so that even stalagmites are strongly affected by the drips (Figure 3c). Interestingly, some corrosion cups are covered with flowstone and contain calcite crystals (RD2 in Figure 3d). Within the Red Hall we have distinguished several areas characterised by different degrees of dissolution and precipitation. These are indicated by red dashed lines in Figure 2c and are explained below:

- Inner corrosion area – contains only cups with bare rock surfaces and corroded speleothems (see examples in Figure 3a, b and c).
- Outer corrosion area – this area encompasses the inner area and contains cups whose upper rim is at least covered in flowstone or which are completely covered by flowstone and often contain broken calcite crystals (e.g., RD2 cup in Figure 3d). Some of the cups in this area are either very slow or inactive.
- Outside the outer area – cups are rare or absent. Some stalagmites have indented tops, but no pronounced corrosion (e.g., RD4). Dissolution takes place only hidden in thin fractures near the floor, through which a high-CO_2 air is introduced during downdraft [15].

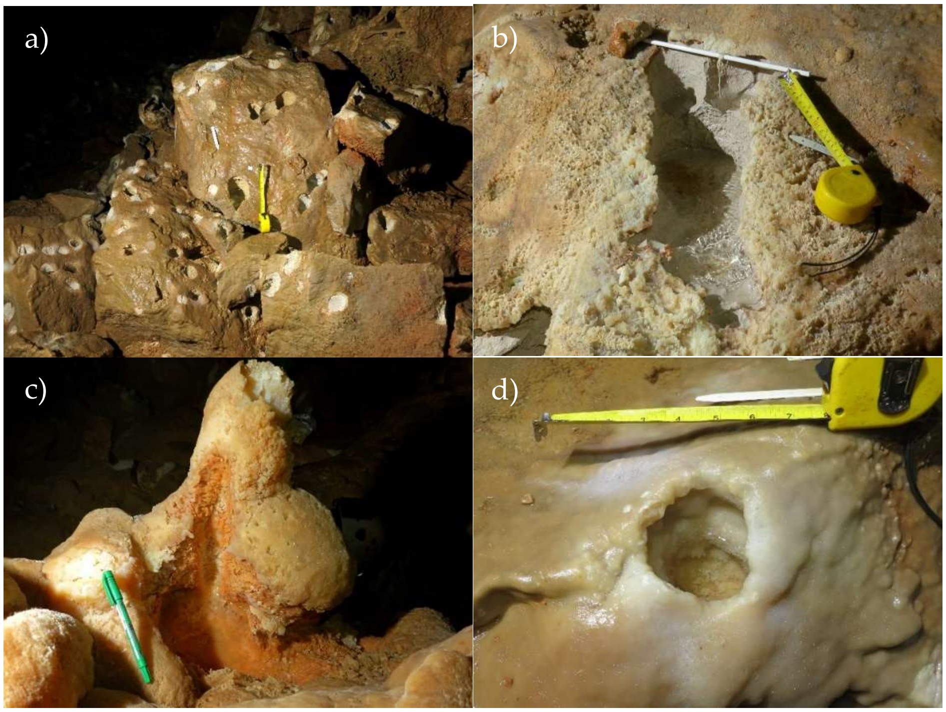

Figure 3. Photos of a selection of corrosion features. (**a**) Boulders in the Red Hall, covered by a thin flowstone crust and corrosion cups. (**b**) Wide shallow RD1 cup with heavily corroded surroundings due to splashing. (**c**) An example of stalagmite that is heavily corroded by several drips. (**d**) RD2 cup covered in flowstone and containing broken crystals. A yellow ruler with a length of ~10 cm or a 14-cm long pen was used as a scale.

2.2. Bedrock Analysis

A rock sample containing two cups was taken from the cave and analysed for its elemental composition (the location in the SC Hall is marked in Figure 2b). The sample contained two cups, one deeper (2 cm) and one shallow (<1 cm), both with grey bare rock surfaces (Figure 4). The rest of the rock surface is covered by a thin crust of yellow flowstone, which in turn is covered by a red flowstone crust. The analysis was carried out with the Agilent 5100 Inductively Coupled Plasma Optical Emission Spectrometer (ICP OES) at the Institute of Geology, Czech Academy of Sciences in Prague. To obtain milligram powder samples, seven distinct spots on the surface were drilled, then dissolved in ~5% HCl and diluted to a 25 mL mark in a volumetric flask. Compositional analysis included the elements: Al, Ba, Ca, Fe, K, Mg, Mn, P, S, Si and Sr. Standard conditions and instrument settings recommended by the manufacturer were used (1200 W RF power, concentric nebuliser, nebuliser pressure 25 psi, sample uptake 2.5 mL/min).

Figure 4. Rock sample with corrosion cups taken from SC Hall in Pisani Passage. Elemental composition samples were taken from seven different locations on the surface marked by pencil marks.

2.3. Dripwater Hydrology

The drip count N was measured with two acoustic Stalagmate® drip counters [42], whose positions were relocated occasionally to cover a wide range of dripping regimes. Occasionally, the drip count was measured manually with or without measuring the drip discharge Q_{drip} (mL/s) directly with a graduated vial and a stopwatch. For slow drip sites where only drip counting was practical, the discharge was calculated from the empirical function between the drip interval Δt and the drop mass m_{drop} reported in the literature $m_{drop} = m_0 + S\Delta t^{-0.75}$ [43]. The function fitting parameters m_0 and S were obtained by comparing data points where both drip discharge and drip count N were measured, with the drop mass calculated as $m_{drop} = \frac{\rho_w Q_{drip} t}{N}$, where ρ_w is the water density (1 kg/dm^3) and t is the time period. Finally, the missing dripwater discharge was then calculated as $Q_{drip} = \frac{N m_{drop}}{\rho_w t}$. The same equation was used to calculate continuous series of drip discharges from drip counts obtained from Stalagmates.

To evaluate the contribution of precipitation to recharge of drips in Pisani Passage, a "water balance" (WB) was calculated by subtracting precipitation from evapotranspiration on a monthly basis.

2.4. Cave Air Monitoring

Continuous monitoring of the cave climate at Postojna Cave includes pCO$_2$, ambient air temperature and airflow velocity. Details of this monitoring setup can be found in a previous publication [15]. In the Red Hall, pCO$_2$ was measured at two levels—one probe was located on the ceiling, directly above the inner corrosion area of the Red Hall, and the other probe was located above the floor at a distance of 20 m and 6.5 m below the ceiling

Preprints (www.preprints.org) | NOT PEER-REVIEWED | Posted: 1 October 2021 doi:10.20944/preprints202110.0008.v1

probe, outside of the area affected by corrosion (Figure 2c). Ambient air $p\mathrm{CO_2}$ in the immediate vicinity of the water sampling sites was measured with Vaisala GM70 portable $\mathrm{CO_2}$ metre using GMP222 or GMP252 probes (compensated at 25°C; measuring range 0–10,000 ppm; resolution 1 ppm for GM252 and 10 ppm for GM222).

2.5. Water Sampling and Monitoring

Water sampling in PP took place at irregular intervals from winter 2017 to summer 2021, with a total of 295 samples collected either in the form of dripwater (drip), water in corrosion cups (cup), flowstone pools (pool) or from a plastic bucket without contact with limestone (bucket). The sampling sites were divided into several groups:

- RD group – drips and their associated cups located in the most corroded area in the Red Hall,
- RD control group – drip that falls on an actively growing stalagmite (RD4) or a calcite pool near the Red Hall,
- PP control group – drips scattered across the PP and not reflecting extreme $p\mathrm{CO_2}$ conditions) and,
- SC Hall group – drip spot in the SC Hall.

Samples of the cup water were collected and filtered with a syringe through a 0.45 μm filter (Acrodisc®) into 60 mL airtight HDPE bottles, while the dripwater was first collected in larger acid-washed bottles and then treated in the same way as the cup water. For the determination of solute concentrations, the water samples were filtered into 15 mL centrifuge tubes. SEC and pH were measured immediately before sampling using a portable multiparameter metre (WTW MultiLine® Multi 3620 IDS) with corresponding probes for measuring pH (WTW SenTix® 940; accuracy ±0.004) and SEC (WTW TetraCon® 925, resolution 1 μS/cm; accuracy ±0.5% of reading; compensation at 25°C), both calibrated in the laboratory before each sampling trip. Both probes are equipped with temperature sensors (accuracy ±0.1°C).

The temporal dynamics of hydrochemistry in cups were recorded by two conductivity loggers with a resolution of 10 minutes (HOBO U24-001, Onset Computer; accuracy ±5 μS/cm). The loggers were immersed in two cups the RD conductivity cup (RD Cond., for 3.5 years) and the RD7 cup (for 1 year). With compensation to 25 °C, the specific electroconductivity (SEC) was obtained and drift was corrected regularly by manual measurements with a calibrated handheld device WTW MultiLine® Multi 3620 IDS. In cases when the cups were dry, erroneous data were removed from the total data set.

2.6. Analytical Methods

The chemical analyses of the water samples were carried out in the laboratory of the Karst Research Institute ZRC SAZU (IZRK) in Postojna and included the measurement of alkalinity, total hardness, calcium hardness and the concentration of major aqueous species. Carbonate alkalinity was determined by potentiometric Gran titration with standardised 0.02 M HCl. All samples for alkalinity were analysed within 48 hours of sampling and stored in a refrigerator prior to analysis. Total and calcium hardness were determined by complexometric titration with 0.01 M EDTA using different buffers and indicators. The Mg concentration was obtained as the difference between the two hardness values. Samples from March 2020 were titrated with the TitroLine 7800 automatic titrator (SI Analytics), using a pH probe A 162 IDS for alkalinity and calibrated before each use.

Initially, the concentrations of the major ions were determined using Shodex YK-421 ion chromatography (IC) in the laboratory of the University of Nova Gorica. However, due to unexpected difficulties with the instrument, the results were erroneous and unusable. In order to be able to use the quantities measured or analysed with other techniques, such as alkalinity, the Ca concentration was estimated using linear correlations. In 2021, the samples were analysed for the concentration of the major ions using the ion chromatograph Metrohm Eco IC, located in the laboratory of the Karst Research Institute ZRC

SAZU. The ion chromatograph consisted of two units for anion (Metrosep A Supp 17 anion column) and cation exchange (Metrosep C 6 cation column) with a self-regenerating suppressor. Concentrations were determined with a conductivity detector and calibrated with standard ion solutions. Determined ions were: Ca^{2+}, Mg^{2+}, Na^{+}, K^{+}, NH_4^{+}, Li^{+}, Cl^{-}, F^{-}, Br^{-}, NO_3^{-}, NO_2^{-}, SO_4^{2-} and PO_4^{3-}. In the analysed samples (n = 18), Li^{+}, PO_4^{3-}, F^{-}, and Br^{-} were below the detection limit.

The derived hydrochemical parameters (saturation index with respect to calcite (SI_{cc}), $p\mathrm{CO}_{2(eq)}$ and $p\mathrm{CO}_{2(sat)}$ ($p\mathrm{CO}_{2(eq)}$ value of water with $SI_{cc} = 0$) for forward and backward mass-balance modelling were calculated using the speciation software PHREEQC [44]. Input parameters included pH, alkalinity, ion concentrations and temperature. The samples that had a charge balance of >5% were discarded for further evaluation. Overall, 89% of the samples were within 5% and 98% within 10% charge balance error.

3. Results

3.1. Bedrock Chemistry

The results of elemental analysis of rock samples containing corrosion cups are given in

Table 1. The composition of the bare rock samples (Rock #1–#4) is typical of pure limestone, while in the flowstone samples there is a depletion of Mg and an enrichment of Na, K and other trace elements. The concentrations of Ba and Mn were below the detection limit (<0.001 ppm and <0.0001 ppm, respectively). The results are comparable to previous chemical analyses of rock or sediment samples in the Pisani Passage [45].

Sample	Ca	Mg	Na	K	S	Fe	Al	Si	P
Rock #1	97.96	0.89	0.42	0.25	0.26	0.07	0.06	0.07	0.00
Rock #2	97.75	0.82	0.56	0.20	0.33	0.12	0.13	0.09	0.00
Rock #3	97.68	0.91	0.56	0.45	0.22	0.04	0.05	0.09	0.00
Rock #4	97.87	0.82	0.43	0.34	0.24	0.04	0.09	0.16	0.00
Flowstone - yellow #1	99.23	0.08	0.25	0.19	0.09	0.04	0.04	0.04	0.03
Flowstone - yellow #2	98.94	0.08	0.37	0.25	0.17	0.07	0.06	0.05	0.01
Flowstone - red	97.86	0.09	0.71	0.58	0.31	0.13	0.16	0.16	0.00

Table 1. Elemental composition of surface features of a rock sample containing corrosion cups. The units are mass percentage per sample.

Sample	Ca	Mg	Na	K	S	Fe	Al	Si	P
Rock #1	97.96	0.89	0.42	0.25	0.26	0.07	0.06	0.07	0.00
Rock #2	97.75	0.82	0.56	0.20	0.33	0.12	0.13	0.09	0.00
Rock #3	97.68	0.91	0.56	0.45	0.22	0.04	0.05	0.09	0.00
Rock #4	97.87	0.82	0.43	0.34	0.24	0.04	0.09	0.16	0.00
Flowstone - yellow #1	99.23	0.08	0.25	0.19	0.09	0.04	0.04	0.04	0.03
Flowstone - yellow #2	98.94	0.08	0.37	0.25	0.17	0.07	0.06	0.05	0.01
Flowstone - red	97.86	0.09	0.71	0.58	0.31	0.13	0.16	0.16	0.00

3.3. Dripwater Hydrology

According to the drip hydrology classification of Baker et al. [46], most of the sampled drips belong to the “seasonal drips” category, while a few others belong to the “subcutaneous flow” or “seepage flow” groups (Figure 5). In the Red Hall, RD1 and RD4 show the greatest variation and the highest discharge rates, but such drip sites are usually rare. The control drip BL2 showed the highest stability of the discharge. Storm events are recorded at virtually every site, and the response depends on the previous saturation of the vadose zone (Figure 6a and b; [47]). Figure 6b shows the responses to precipitation at some continuously monitored drip sites (RD1, RD5 and RD7), while Figure 6c compares the drip discharge with continuous variations in SEC in cup water and $p\text{CO}_2$ in cave air near the floor.

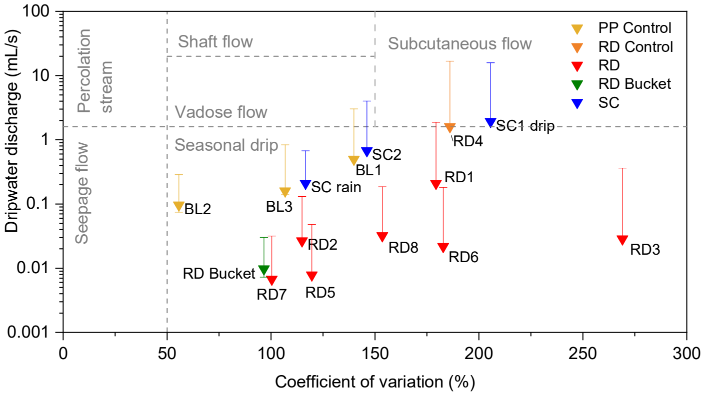

Figure 5. Classification of drip spot based on manual measurements of drip discharges following Baker et al. [46]. Symbols denote averages, whiskers denote ranges.

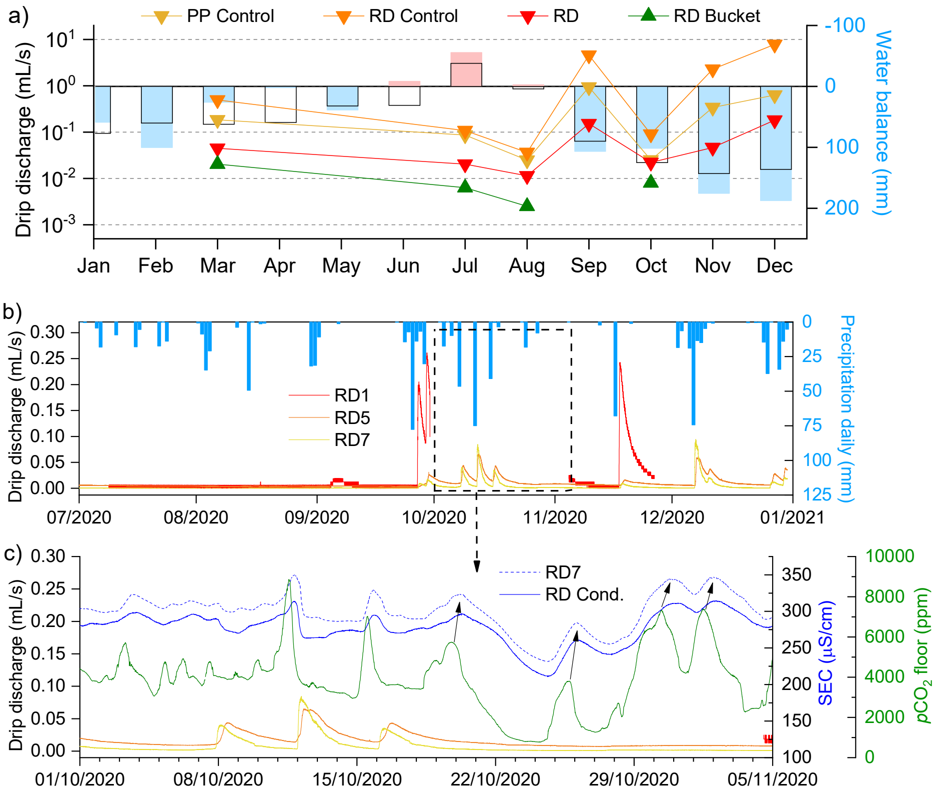

Figure 6. (**a**) Time series of drip discharge and water balance on a monthly basis. The blue and red columns show the positive and negative water balance (excess or deficit, respectively), calculated as the difference between precipitation and net evapotranspiration (calculated with the Penman-Monteith equation) [37]. The black boxes show the climatic averages (1981–2010). (**b**) A 6-month window of drip response to precipitation events (blue bars; on a daily scale). The seepage flow with a fracture-fed component is represented by RD1 (red curve), while the seepage flow with a typical diffuse component is represented by RD5 and RD7 (orange and yellow curves). Both diffuse drips did not respond to summer precipitation, while RD1 showed a very low response. Precipitation data are from the Postojna national meteorological station, located 2.5 km SSW of Pisani Pas-

sage [37]. (**c**) Inset from (**b**) showing higher resolution in a shorter time frame with continuous electroconductivity (SEC) from RD Cond. and RD7 cups (dashed and solid blue curves) and pCO_2 at the cave floor (green line). The lag time between the pCO_2 peaks and the response to the SEC peaks ranges from a few hours to about 12 hours (marked by black arrows).

During the monitoring period 2017–2020, the mean annual precipitation was 1596 mm, close to the climatic mean (1500 mm). Precipitation was concentrated in the cooler period, with the wettest months Sept, Nov and Dec receiving 125% of the usual (climatic) precipitation, while the three driest months Jan, Mar and Apr received 80% of the usual amount (Figure 6a). Dripwater discharge followed the seasonal trend of precipitation, with the highest discharges occurring in the wetter, cooler months (especially autumn), when the water excess is greatest. In summer (Jun–Aug), all monitored drips in the Red Hall except RD4 dried or became very slow (~2 drips/min), which was the main limiting factor for sampling during this period. The longest period of above-average precipitation was winter 2017–2018 (Nov 2017–Apr 2018; 38% more precipitation), exactly during the first and most frequent water sampling trips.

3.3. Spatiotemporal Dynamics of CO_2

The spatial and temporal CO_2 dynamics in the Pisani Passage have been investigated in a previous study [15], while only the results relevant to the geochemistry of the dripwater are reviewed here. The CO_2 dynamics follow the seasonal airflow pattern for Postojna Cave, with the highest pCO_2 values measured in warm periods (Jul–Sept) when the downdraft prevails, and the lowest in cooler months (Dec–Feb) during the updraft, when values often approach those outside (Figure 7). In cooler periods, air moves through large airflow pathways (direction from the main entrance towards PP), while in warm periods air is directed from the soil and the vadose zone with high pCO_2 to the interior of PP (see airflow direction in Figure 2a). High CO_2 conditions in winter occur only exceptionally when NE winds force the ventilation direction into downdraft and last only for a short time [48]. In the Pisani Passage pCO_2 values gradually increase from about 1000–2000 ppm to about 3000–4000 ppm from the entrance toward the farthest extent. The greatest increase in pCO_2 is found in the lowest floor sections of Red Hall and White Hall at the end of Pisani Passage (Figure 2b). Where the air is sheltered from ventilation and mixing, a pCO_2 value of 12,640 ppm was measured, which is not only the maximum value of Pisani Passage, but also of Postojna Cave. Due to the different characteristics and positions of the airflow pathways, the air in the Red Hall is stratified, with pCO_2 values near the floor showing ~6000 ppm higher values than at the ceiling in extreme cases. This contrast is illustrated by the 2017–2020 time series in Figure 7 with green shading. The stratification of the air is supported by a downdraft, while an updraft mixes the air and homogenises the distribution of CO_2 [15].

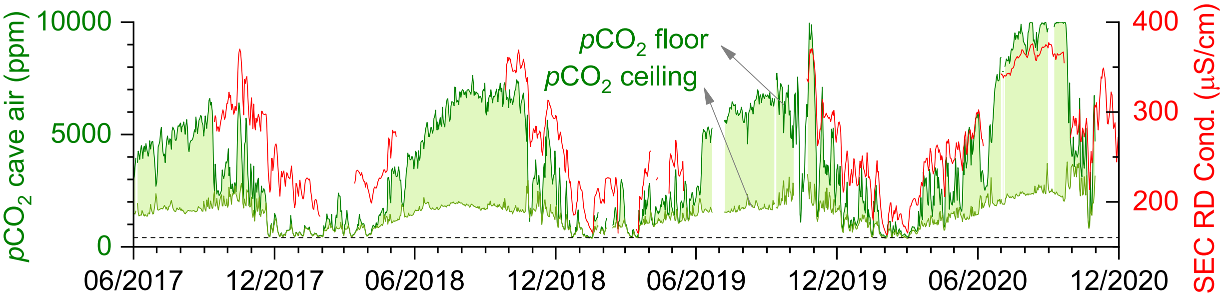

Figure 7. Time series of daily pCO_2 fluctuations in Red Hall at floor (dark green) and ceiling (light green) compared to SEC (red line), measured in the RD Cond. cup. The green shading represents the difference in CO_2 concentration between the floor and the ceiling of the Red Hall.

3.4. Drip and Cup Water Chemistry

As mentioned in the methods section, most of the samples analysed using Shodex YK-421 IC gave erroneous major ion concentrations. In order to be able to use the data nevertheless, Ca was calculated using a strong linear relationship with alkalinity determined by a separate method, i.e. potentiometric titration. The relationship is shown in Figure 8 and is evaluated by the Pearson factor ρ (0.9982) and the coefficient of determination R^2 (0.9963). The linear relationship was also consistent with the theoretical line, confirming that the sampled waters were predominantly Ca-HCO_3 type. The Mg concentration showed a weak correlation with alkalinity, so a constant value of 0.04 mmol/L was used, which is also the mean value of the Mg concentration determined in the subsequent analyses. Possible fluctuations and deviations of Mg from this value proved to be insignificant for the further interpretation of the results and previous studies confirm that this is a reasonable estimate [41].

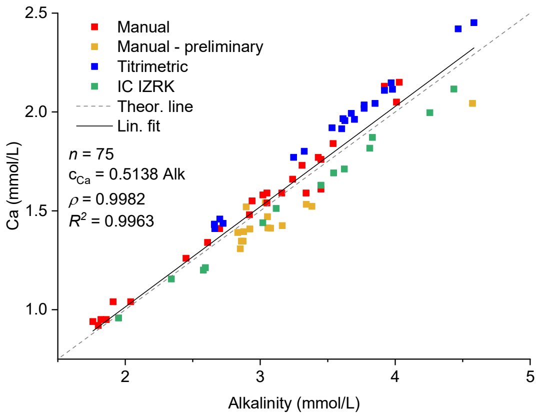

Figure 8. Linear correlation between Ca concentration and carbonate alkalinity for samples where Ca concentration was measured manually, titrimetrically or via IC at IZRK. The linear relationship was used to calculate the Ca concentration in incorrectly analysed samples. The similar slope of the theoretical line (pure $Ca(HCO_3)_2$ solution; dashed line) and the fitted line (solid line) confirms that the water samples are indeed mostly of the Ca-HCO_3 type, regardless of the sampling site or the time period of sampling. However, a positive deviation of the Ca concentration can be seen in the samples analysed with the titrimetric method and a negative deviation in the samples analysed with the IC, the cause of which is unknown.

Time series of alkalinity, calcium concentration, SEC, pH, SI_{cc} and pCO_2 of cave air were summarised as collated monthly averages over the period 2017–2020 (Figure 9). All parameters show seasonal variations with few exceptions (see discussion in section 4.2.1.). In the cooler months, dissolved ion concentrations are lowest, while pH and SI_{cc} values are highest. In the warm summer months, the samples have higher solute loads (alkalinity, Ca and SEC) and a wide range in SI_{cc} (from –0.5 at RD to 0.5 at the control sites). The control drips are the least variable, showing almost constant values for Ca, alkalinity and SEC, but show minor fluctuation in pH and SI_{cc} like other sites. The SI_{cc} value of the control drips never falls below zero. The average value of alkalinity is highest in the control drips at PP (4.3 mmol/L) and much lower in the RD drips (2.8 mmol/L). Similar extremes are found for Ca concentration (2.2 mmol/L for the control group to 1.5 mmol/L for the RD drips) and SEC (from 389 µS/cm to 291 µS/cm). This difference between RD drips and controls occurs throughout the year, regardless of the season, which was already observed in a previous study [41]. When comparing RD drips and cups, the differences in the aqueous species are minimal in the cooler months and maximal in summer (Jul–Aug). The dripwater temperature ranges from 8.7 °C to 9.1 °C, while the average water temperature in the cups is within these values (8.9 ± 0.2 °C), which is again very similar to the average air temperature in RD (8.8 °C) [15].

Preprints (www.preprints.org) | NOT PEER-REVIEWED | Posted: 1 October 2021 doi:10.20944/preprints202110.0008.v1

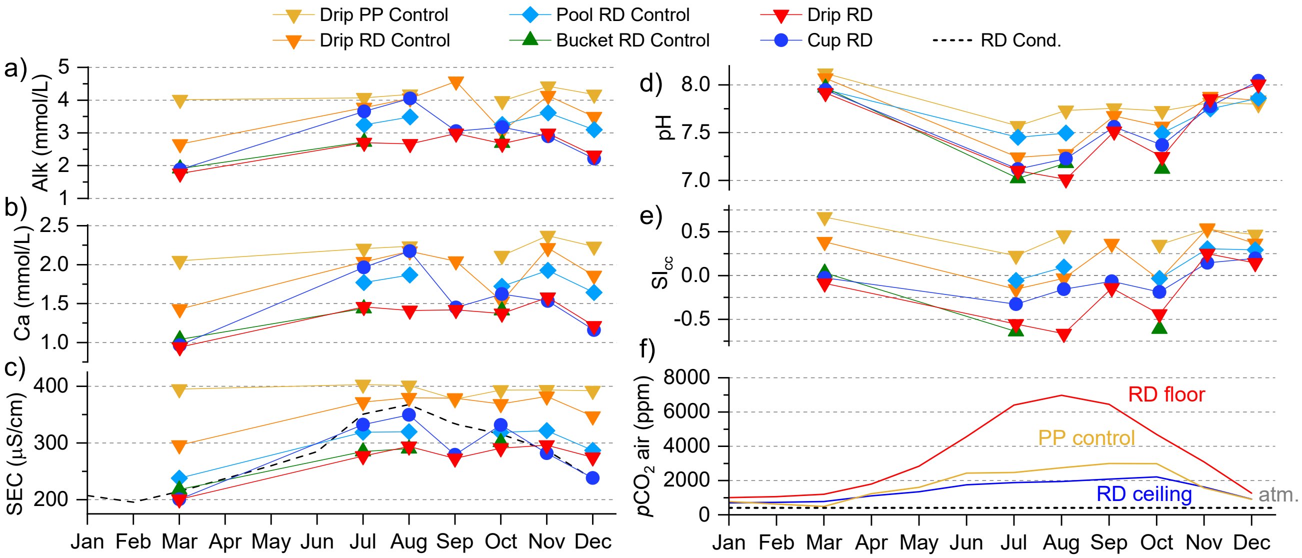

Figure 9. Collated monthly averages of cave air and water data collected during 2017–2020. Time series of alkalinity (**a**), Ca concentration (**b**), SEC (**c**), pH (**d**), SI$_{cc}$ (**e**) and cave air pCO$_2$ (**f**) for different sampling sites in Pisani Passage. The black dashed line in (**c**) shows the values of the continuous records from SEC of RD Cond. cup. Monthly pCO$_2$ values in Red Hall were calculated from continuous time series for the floor and ceiling (Figure 7), while PP represents mean pCO$_2$ values measured manually at PP control sites.

The continuous time series of the RD Cond. cup water SEC closely followed manual measurements in other cup waters, which was confirmed by a high linear correlation (ρ = 0.9951, R^2 = 0.9901). A similar high correlation was found in the case of the neighbouring RD7 cup (ρ = 0.9985, R^2 = 0.9970; also shown in Figure 6c). A high correlation was found between SEC and pCO$_2$ (already shown in Figure 7). Any change in pCO$_2$ is quickly reflected in the water chemistry, which can also be seen in the moderate correlation between log(pCO$_2$) and SEC or pH (Figure 10a and b). The linear correlation between Ca concentration in the water samples and SEC is strong (Figure 10c, ρ = 0.8876, R^2 = 0.7848), which is very similar to the correlation from the global dataset for clean carbonate waters [49]. The linear relationship of SEC with alkalinity of water samples is also strong (Figure 10d; ρ = 0.9115, R^2 = 0.8301). The mean values of the aqueous parameters (Ca^{2+} and HCO$_3^-$ concentrations, pH and SEC), their variations and correlations from Figure 10 are in agreement with previously published results [41,50].

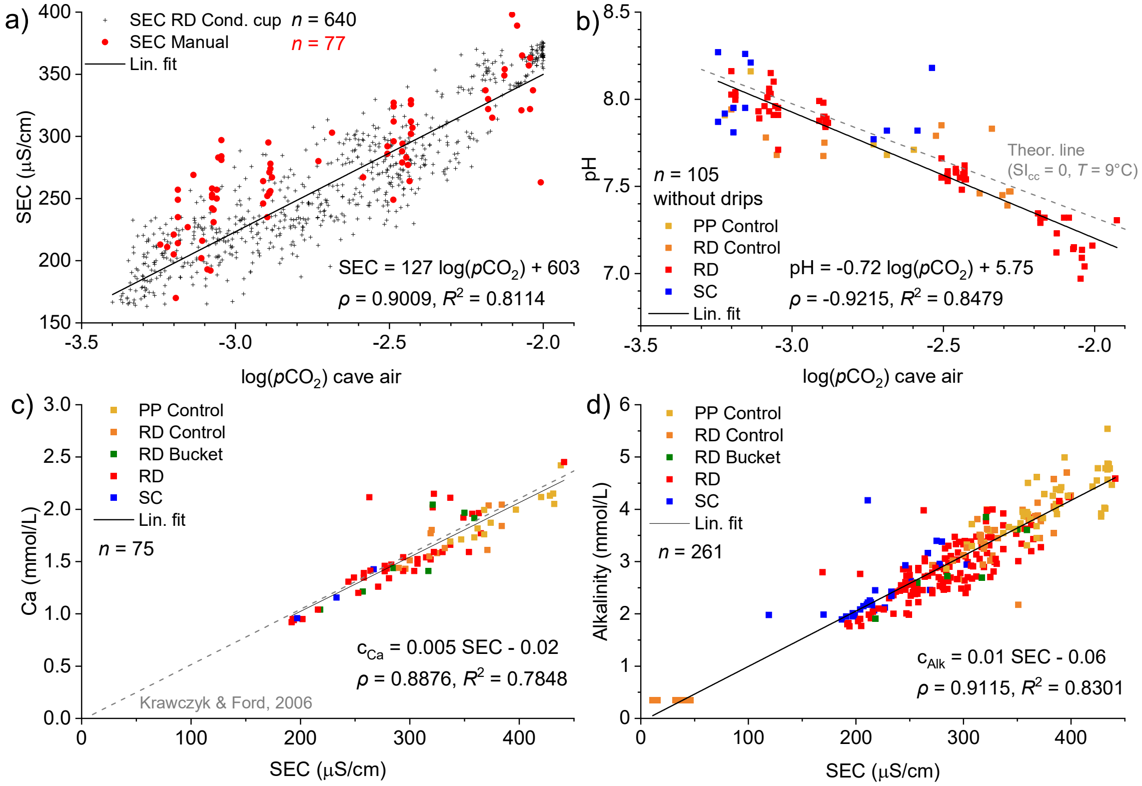

Figure 10. Correlation between log(pCO_2) at the floor and manual or continuous SEC values (**a**) or pH measurements of cup or pool water (**b**). Correlation between electroconductivity and manual calcium concentrations (**c**) or alkalinity (**d**).

4. Discussion

4.1. Origins of Undersaturated Dripwaters

4.1.1. Geology

One of the plausible explanations for the increased dissolution in the Red Hall is a possible susceptibility of the limestone to dissolution due to its impurity content, which could cause increased acidity in addition to the usual carbonic acid dissolution. The results of elemental analysis of a single rock block with a corrosion cup (Figure 4) are given in

Table 1 and indicate that this is not the case. The rock is indeed composed of pure limestone, typical of the lithology of the Pisani Passage, as it likely derives from breakdown of the host rock. Analysis of the flowstone covering the rock sample revealed a similar composition with a depletion in Mg concentration [45]. Considering the vadose zone that determines the chemistry of the percolating water, the lithology is not expected to differ over the extent of the cave to the surface [34]. Our results and previous dripwater

Sample	Ca	Mg	Na	K	S	Fe	Al	Si	P
Rock #1	97.96	0.89	0.42	0.25	0.26	0.07	0.06	0.07	0.00
Rock #2	97.75	0.82	0.56	0.20	0.33	0.12	0.13	0.09	0.00
Rock #3	97.68	0.91	0.56	0.45	0.22	0.04	0.05	0.09	0.00
Rock #4	97.87	0.82	0.43	0.34	0.24	0.04	0.09	0.16	0.00
Flowstone - yellow #1	99.23	0.08	0.25	0.19	0.09	0.04	0.04	0.04	0.03
Flowstone - yellow #2	98.94	0.08	0.37	0.25	0.17	0.07	0.06	0.05	0.01
Flowstone - red	97.86	0.09	0.71	0.58	0.31	0.13	0.16	0.16	0.00

analyses carried out at Pisani Passage show that the dripwater is of the Ca-HCO_3 type characteristic of water percolating through pure carbonate karst [45]. We might expect a greater influence on water chemistry at SC Hall, where dolomitised limestone and chert lenses have been detected [38,51,52]. However, our hydrochemical results, which we present in the following sections, do not support this assumption either. More interestingly, the vadose zone above Pisani Passage has a variable thickness, with the greatest cover at the entrance (~100 m), gradually decreasing to 50 m above SC Hall and to 30 m above Red Hall as the passage approaches the Jeršanova Doline, which terminated the course of the passage to the north [35,51]. Many hydrochemical parameters of the sampled drips show a trend related to this reduction in the thickness of the vadose zone along the Pisani passage, which is explained in more detail in the following chapter.

4.1.2. Soil and Vadose Zone Conditions

To explore the possible origin of the undersaturated dripwater, backward modelling of water chemistry could provide an estimate of pCO_2 in the vadose zone before the water equilibrates to cave conditions. However, this value will always be an underestimate due to the possibility of PCP, incomplete saturation, closed system conditions or incomplete soil cover [29,30,53]. In a diagram showing the relationship between Ca concentration and log(pCO_2) (Figure 11), it is clear that the different drip groups occupy different areas. In general, the control drips have higher Ca concentrations than the drips causing corrosion, while the Ca concentrations of the corrosion cup water tend to lie between these two groups. Under the open system conditions, the maximum possible pCO_2 value of the water in equilibrium with the gas phase, i.e. $pCO_{2(eq)}$, for the control group of drips is about $10^{-1.6}$ (~25,000 ppm; black arrows), while the minimum value for the same group is about $10^{-2.2}$ (~6300 ppm). For the RD drips that result in corrosion and the cup waters, the maximum value is obtained to be $10^{-2.0}$ (~10,000 ppm; black dashed arrows), while the minimum value is $10^{-3.1}$ (~800 ppm), but such low values tend to indicate strong degassing in the cave before collection, usually in winter. The highest Ca concentrations would thus be explained by the parent solution being in contact with the highest pCO_2 of the vadose zone, as was found to be the case with the PP control group.

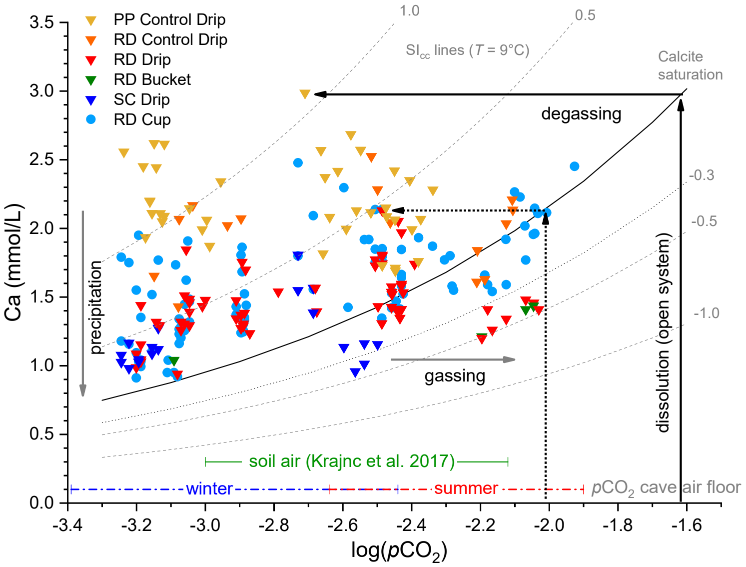

Figure 11. Water chemistry evolution for drip and cup water samples collected at Pisani Passage. The grey curves denote constant SI_{cc} values at T = 9 °C. The arrows show the direction of the dominant processes in the carbonate water chemistry. Explanations can be found in the text. The green line marks the log(pCO_2) range measured in the soil, while the blue and red dashed lines mark the winter and red ranges, respectively.

Monitoring soil pCO$_2$ may provide another boundary for evaluating the formation of initial dripwater chemistry. The only such study to date, where the monitoring setup was located at the surface directly above the Red Hall, was conducted by Krajnc et al. [40] in 2014–2015. There, it was found that the seasonal dynamics of pCO$_2$ and δ^{13}CO$_2$ in the soil at different soil depths (20–80 cm) were promoted by cave ventilation, in contrast to the typical factors of soil temperature and soil water content that control soil CO$_2$ production at a nearby control site. The pCO$_2$ value in the soil ranged from 1000 to 7600 ppm, which was lower than the maximum value measured in the cave (10,426 ppm; the pCO$_2$ range in soil air is marked by a green line in Figure 11). However, the measured soil pCO$_2$ value could be underestimated due to the possible existence of a rich sub-soil CO$_2$ reservoir. Moreover, many other studies suggest that the stronger sources of CO$_2$ are deeper in the vadose zone than in the soil zone and epikarst, where biogenic CO$_2$ production is expected to be greatest [8,29,54–56]. Accordingly, the high CO$_2$ zone in our case seems to be shifted even deeper into the cave itself [15]. Also, soil cover was not found to be important factor in determining water chemistry, as it does not vary across the extent of PP on the surface [53]. Surface cover is generally uniform with rocky soils in forested areas.

4.1.3. Thickness of the Vadose Zone

Comparing the results of the different sampling groups in Figure 11 with the morphology of PP (Figure 2b), there appears to be a negative trend in Ca concentration and distance from the PP entrance. The geochemical profile in Figure 12a shows that this trend can also be related to the thickness of the vadose zone, which, as mentioned earlier, decreases from the entrance to the end of PP. To confirm this influence on the initial dripwater chemistry, we sampled additional water samples across PP on 14 July 2021. The results are shown in Figure 12b and c. The Ca concentration of the dripping water indeed decreases with distance from the entrance of the PP or with decreasing thickness of the vadose zone. The Ca concentration of the dripwater decreased from about 2 mmol/L measured near the entrance of the passage to as low as 1.2 mmol/L in the Red Hall. The exceptions are in the SC Hall, where the lower Ca (<1.2 mmol/L) is probably due to a more direct connection to the surface, and in BL3 with a higher Ca concentration (>2 mmol/L), perhaps due to much longer water pathways. The correlation was moderate but surprisingly high when considering all possible factors that could influence water chemistry (e.g. varying pCO$_2$ in the soil or vadose zone, water flow pathways, airflow pathways, open or closed system conditions).

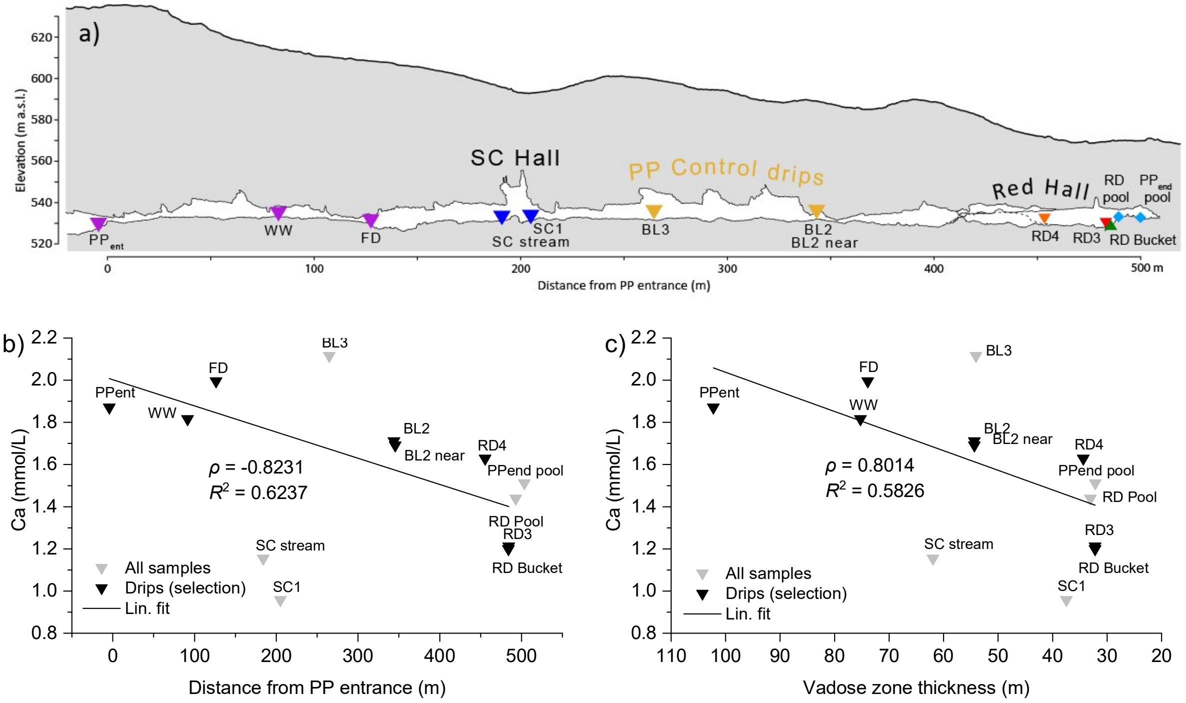

Figure 12. (**a**) Schematic profile of the Pisani Passage showing the sites sampled during the single occasion on 14 July 2021. The profile of the surface was acquired from LiDAR scans and follows the extent of the passage [37]. (**b**) Relationship between the calcium concentration in the dripwater and the distance from the entrance of Pisani Passage or (**c**) the thickness of the vadose zone determined by the LiDAR digital elevation model. Note the inverted X-axis in (**c**). Samples BL3 and SC are considered outliers and were not included in the calculation of the linear regressions.

4.2. Processes Occuring in the Cave

4.2.1. Dripwater Entering the Cave Atmosphere

Drip discharge is greatest in cooler months—during periods of increased water excess (Figure 6a) and shortly after heavy precipitation events (>20 mm/day; Figure 6b). In warm months, many of the drip sites dry up at Red Hall or reduce to constant low drip rates of about 2 drips per minute and do not respond to precipitation events. For two of the longest available time series of drip counts, a moderate correlation was found between discharge rate and water balance on a monthly basis (R^2 = 0.5372 for RD5 and R^2 = 0.6438 for RD7). This behaviour can be explained by the saturation of the vadose zone, which replenishes during the cooler period and depletes during the warm period when evapotranspiration increases [1,57]. In the Red Hall, only a small percentage of drip sites show fracture-fed seepage (e.g. RD1 in Figure 6b), while the majority of drips are fed by the slow draining matrix component. After precipitation, the majority of RD drips show a sharp increase in SEC (Figure 6b); a response that contrasts with the rapid fracture-fed sites where a decrease in SEC and undersaturation with respect to calcite is probable. However, the variations in SEC correlated more with changes in $p\mathrm{CO}_2$ in the cave air than with hydrology (see time series in Figure 7 and the correlation in Figure 10a). This was also true for SI_{cc}, which correlated only weakly with drip discharge. Compared to the RD drips above the corrosion cups, the PP control drip group showed lower annual fluctuations in drip discharges, stable water chemistry with almost constant SEC and generally higher solute concentrations (Figure 9). All PP control drips had positive SI_{cc} values throughout the year, with the maximum occurring in winter (Figure 9e). Such behaviour of these sites could indicate efficient buffering of the outside signal, which could be related to the thicker vadose zone above these sites than above Red Hall.

doi:10.20944/preprints202110.0008.v1

We now discuss whether the kinetics of carbonate chemistry could play an important role in determining the geochemical conditions in the Red Hall. The initial degassing of dissolved CO_2 from solution occurs within seconds, while the subsequent equilibration with an increase in pH and SI_{cc} is an order of magnitude slower as HCO_3^- is converted to CO_2 [31]. Therefore, slow drips with drip interval longer than the initial degassing phase would be most likely equilibrated to the low pCO_2 at ceiling level and achieve the greatest supersaturation. However, without further precipitation at the ceiling, no change in calcium concentration can be expected between a drip sampled at the ceiling and a drip sampled near the floor. Only very slow drips (drip interval in the range of ~400 s) would exhibit precipitation, i.e. PCP. None of our samples show such slow drips, not even in dry summer periods. From visual inspection of the ceiling, we concluded that precipitation does not readily occur at the ceiling. However, PCP could be important as many of the geochemical parameters resulting from this process are found in our data (low SEC, low SI_{cc} and low mineralisation; [58]). However, to diagnose PCP, at least the ratios of trace elements (e.g. Mg/Ca and Sr/Ca) and the $\delta^{13}C$ signature would need to be determined, with higher values being a key signal for this process. Mixing corrosion as a source of potential dissolution in the Red Hall might also play a role [58], but this scenario, as well as PCP that would have to take place in the vadose zone, are highly unlikely to control the geochemistry in our case, as there is simply an abundance of corrosion features over a wider area fed by several hundred different drips.

4.2.2. Dripwater Evolution in the Cave

The dripwaters that emerge at the control sites of PP and RD almost always originate from an atmosphere with similar or higher pCO_2 than in the cave. This is illustrated in Figure 13 by the monthly variations of pCO_2 in the cave air and $pCO_{2(sat)}$ in the water ($pCO_{2(eq)}$ of the solution forced to $SI_{cc} = 0$). The maximum value of $pCO_{2(sat)}$ obtained for the controls from RD is close to the maximum value measured in the cave (~12,000 ppm). In contrast, the RD drips above the corrosion cups appear to have lower $pCO_{2(sat)}$ values than the cave air pCO_2 value, especially in the warm period (Jul–Sep), as indicated by the red shading in Figure 13. In the period Jul–Aug, such a geochemical situation was also observed at the sites in the SC Hall. Interestingly, none of the drips, neither RD nor the control, show a stability of $pCO_{2(sat)}$, but show a similar seasonality as the pCO_2 of the cave air. One of the reasons for this could be that the dominant sources of CO_2 are located in the soil zone and epikarst, where surface conditions vary with the seasons and hydrological conditions. Another explanation could be strong degassing along water flow paths and the possibility of PCP, either in the vadose zone or at the ceiling. This could be the case if drips do not fall directly on the stalagmite but flow along the outside of the stalactites or along the cave walls, and even more so if the drip interval is long [28,31,59]. The range of estimated $pCO_{2(sat)}$ values at Red Hall is consistent with the recent study in which the $pCO_{2(sat)}$ value of dripwater sampled at Pisani Passage near RD (8710 ppm) was the lowest of all drip sites studied at Postojna Cave, although the highest pCO_2 value of cave air was measured there [32]. Using the data published by Vokal et al. [50] for the measurement site in the SC Hall, we again calculated a similar range of $pCO_{2(sat)}$ as in our control or SC measurements (2800–5500 ppm).

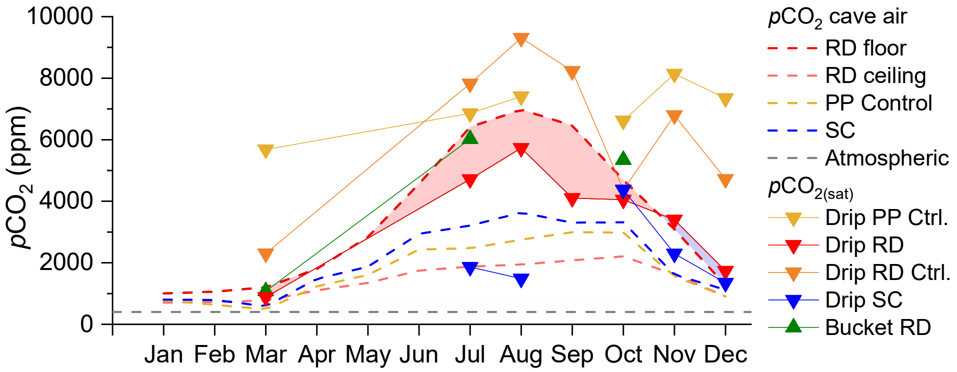

Figure 13. Variation in $pCO_{2(sat)}$ values ($pCO_{2(eq)}$ of solution forced to $SI_{cc} = 0$; solid lines) for different drips in the Pisani Passage compared to the pCO_2 dynamics of cave air in the Red Hall on a monthly scale (dashed lines). The red shading indicates the range of potential dissolution in the Red Hall, while the blue shading indicates precipitation.

In the Figure 14, comparing the dripwater SI_{cc} and log(pCO_2) values, the majority of the drip groups lie along degassing or gassing lines (slope ~–1), assuming a possible wide range of $pCO_{2(sat)}$ between $10^{-3.0}$ (1000 ppm) and $10^{-1.8}$ (~16,000 ppm), and are assumed to originate from parent solutions with $SI_{cc} = 0$ [59]. The scatter between sites can be explained by different water flow paths, conditions in the vadose zone and PCP. As expected, the highest calcite saturation (~0.8) is reached in the control group. RD drips reach $SI_{cc} \approx 0.6$ only in cooler months, while above a cave air pCO_2 value of $10^{-2.2}$ (~6300 ppm) they exclusively show undersaturation.

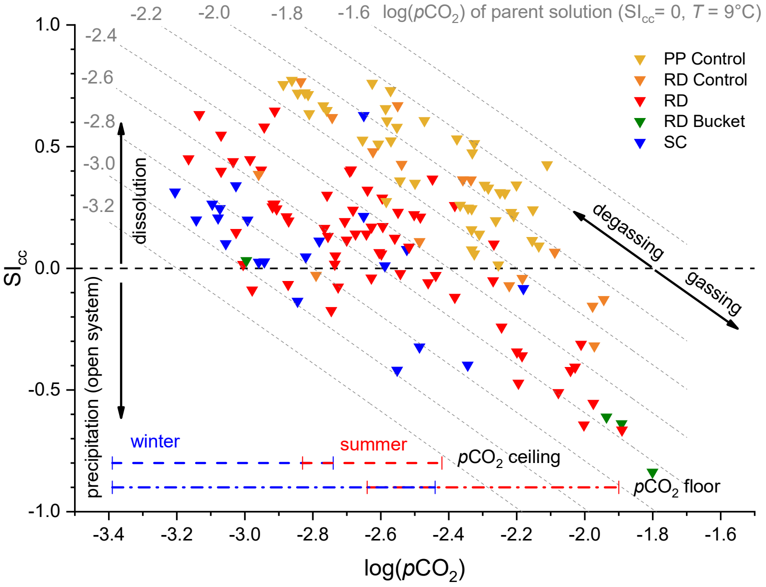

Figure 14. Dripwater SI_{cc} in Pisani Passage as a function of log(pCO_2). The grey lines denote the processes of gassing or degassing from parent solution (assuming $SI_{cc} = 0$, $T = 9$ °C) and range from log(pCO_2) = –3.2 (~630 ppm) to log(pCO_2) = –1.6 (~25,000 ppm). The measured ranges of cave air pCO_2 are marked by dashed lines for winter (blue) and summer (red) for the ceiling and floor CO_2 probes. Note that at a cave air pCO_2 of $10^{-2.2}$ (6300 ppm), the RD drips associated with the corrosion cups fall exclusively in the undersaturated area.

4.2.3. Mechanism of Cup Formation

Seasonal cave ventilation, driven by the chimney effect, controls the temporal dynamics of pCO_2 in cave air [15]. The clearest link between pCO_2 in cave air and water chemistry comes from records of electroconductivity (as explored in detail in [60]). The continuous time series of SEC measured in the RD Cond. cup showed high similarity with all other manually measured SEC values in the Red Hall (see red dots in Figure 10a), resulting in a high correlation coefficient ($\rho = 0.9951$, $R^2 = 0.9901$). Thus, although fed from different infiltration pathways, the differences in SEC are small when comparing different cups within a given time period. Moreover, the cup water SEC shows a very high similarity with the variation of pCO_2 in Red Hall (Figure 7 and a closer view in Figure 6c). Although Red Hall is characterised by a vertical gradient of pCO_2 in the air, the pCO_2 at the floor level—where the cups are located—is uniform and varies little horizontally [15]. The continuous time series of pCO_2 of cave air at the floor station therefore strongly reflects the pCO_2 conditions prevailing in the area of cup formation, while the similarity with the values of SEC suggests a controlling role (as seen in Figure 10a; $\rho = 0.9009$, $R^2 = 0.8114$). As the pCO_2 in the air increases, some CO_2 dissolves in the solution, dissolving the cup wall and forming ions that increase SEC. Conversely, as pCO_2 falls, the water equilibrium shifts back, releasing gaseous CO_2, precipitating calcite and causing SEC to fall. In this way, the seasonal fluctuations in pCO_2 imprints a similar variation in SEC of cup water, with low values in winter (~200 μS/cm) and high values in summer (~300 μS/cm). The response of pCO_2 fluctuation to the chemistry of the cup water is visible on an hourly scale. We found that the delay of the response can be in a wide range from a few hours to about 12 hours (Figure 6c). In the inner RD area of corrosion, precipitated calcite crystals are not clearly visible in the corrosion cups, but in the cups in the outer area, even millimetre-sized crystals can grow, as in the case of RD2 (Figure 2d).

Low initial calcium concentrations of dripwaters in the Red Hall and the SC Hall have an important effect on SI_{cc}, as an increase in pCO_2 in the cave air tends to undersaturate such drips, especially in RD, where CO_2 accumulates [14,16]. This is already illustrated in the theoretical example in Figure 1 by the water evolution from point D to H and is also visible in our case in Figure 11. In the pCO_2 range of $10^{-2.2}$–$10^{-2.0}$ (6300–10,000 ppm), there is a clear difference in Ca concentrations between RD cups (blue dots) and drips (red triangles), with the cups having a concentration about 0.5 mmol/L higher than the drips. Above a pCO_2 threshold of $10^{-2.2}$ (~6300 ppm), the RD drips have an $SI_{cc} \approx -0.3$, while RD cups have a slightly lower $SI_{cc} \approx -0.25$. Since the RD drips are collected directly above the respective cups, they are equilibrated to the high CO_2 conditions prevailing near the cups. When the dripping water comes into contact with the cup walls, dissolution occurs, eventually elevating the SI_{cc} towards zero. RD Bucket shows a similar chemistry to the RD drips in that it is actually a dripwater that is in equilibrium with the pCO_2 at the floor, but unable to dissolve calcite (see RD Bucket in Figure 11). The lowest limit of the pCO_2 at floor, where some drips and cups start to become undersaturated, is already at ~$10^{-2.5}$ (~3200 ppm). Interestingly, cave air pCO_2 values were above this limit exactly 50% of the time during 2017–2020 [15]. The greatest dissolution would be expected in cases where drips and cups were strongly degassed before the pCO_2 value of the cave air increased, as shown in the theoretical example in **Figure 1**. This could be achieved, for example, during summer periods with strong airflow reversals that temporarily deplete pCO_2 of the cave air but quickly re-establish high CO_2 conditions and gradients (see, for example, October 2019 in Figure 7). RD Control drip is less likely to be affected by changes in cave air pCO_2, but shows undersaturation when pCO_2 rises above a similar threshold as before ($10^{-2.3}$, ~5000 ppm). Although high CO_2 levels have been found in both Red Hall and White Hall, large, macro-scale dissolution features are only found in Red Hall, where the dripwaters feeding the cups have generally the lowest Ca concentrations.

In contrast, neither strong fluctuations in pCO_2 nor an air stratification phenomenon were found in the SC Hall (pCO_2 range 450–5100 ppm, average 1800 ppm). There, the ceiling of the SC Hall is much higher and the drip sources are beyond sight, but many drips come from >50 m high chimneys, which could progress even further into the vadose zone.

The largest variations in drip discharges and the lowest measured Ca concentrations indicate a higher proportion of undersaturated fracture flow. Therefore, a higher degree of geological and hydrological control is expected, apart from the dynamics of cave air $p\mathrm{CO_2}$, which does not need to be elevated to achieve undersaturation of dripwater.

4.3. Dominating Controls

The previously proposed and discussed control mechanisms for the formation of corrosion cups are now summarised and the main arguments are further elaborated:

1) The rock overburden becomes thinner towards the end of the Pisani Passage and the Ca concentration of the dripwater is lower in the Red Hall than at the control sites. In such an environment, the $p\mathrm{CO_2}$ of the cave air is more likely to modulate calcite saturation state towards undersaturation. In the SC Hall, water pathways from the surface are probably more direct, which explains the low Ca concentrations in dripwater.
2) In warm periods during downdraft, the floor of the terminal section of Red Hall is sheltered from advection, which promotes $\mathrm{CO_2}$ accumulation, while the ceiling is in an efficient ventilation pathway [15]. In such an environment, the dripping water near the ceiling can easily degas, but more importantly, the $\mathrm{CO_2}$ is absorbed near the floor. The estimated $p\mathrm{CO_2}$ of the percolating water in the vadose zone (i.e. the $p\mathrm{CO_{2(sat)}}$) was always lower than the air $p\mathrm{CO_2}$ measured at the cave floor during warm periods. Such a contrast causes dripwater at the cave floor to become undersaturated, which promotes dissolution of calcite and the formation of corrosion cups.
3) The degree of dissolution is controlled by both the hydrological conditions of the vadose zone and the conditions of the cave air. While high $p\mathrm{CO_2}$ values regularly occur in late summer (Jul–Sep), dripwater discharge is usually lowest at this time. In winter, this behaviour is reversed; the $p\mathrm{CO_2}$ value is low and the discharge rate is increased. In intermediate periods such as autumn or when there are rapid short-term changes in the $p\mathrm{CO_2}$ of the cave air, the fluctuating $p\mathrm{CO_{2(eq)}}$ of the water could be the most important factor for the increased dissolution in the corrosion cups.

As for the second and third points, the Ca concentrations of the RD drip waters, which fed the corrosion cups, vary only slightly (1.5 ± 0.2 mmol/L) within a year, which means that the variations of the dripwater $\mathrm{SI_{cc}}$ are mainly influenced by the variations of the $p\mathrm{CO_2}$ of the cave air. Of course, the highest dissolution is expected in the warm summer, but in parallel, the dripwater discharge becomes the limiting factor. Since dripping is increased in cooler periods, we would assume that late summer (still warm, downdraft ventilation, high $p\mathrm{CO_2}$) and early autumn (increased saturation of the vadose zone) are the periods with the most intense dissolution. This is likely to be true to some extent, as our data show, for example, that the onset of a wet period quickly dilutes the cups with fresh water, regardless of the high $p\mathrm{CO_2}$ in the cave air. This can be seen in Figure 9e for the RD cups in September, when the $\mathrm{SI_{cc}}$ increases with increasing precipitation (rainfall). The pre-summer dissolution is probably most intense in spring, when the water contained in the cups is most degassed and the Ca concentration in dripwater reaches a minimum, so the $p\mathrm{CO_{2(eq)}}$ change is greatest with the onset of the summer downdraft and the increase in cave air $p\mathrm{CO_2}$. Further research is needed to better constrain the timing of dissolution and its hydrological control through more frequent sampling and measurement of drip rate during a single hydrological year.

4.4. Dissolution Rate Estimates

The hydrochemical results and the comparison with the cave air dynamics reveal control and temporal dynamics of the formation of corrosion cup, but there are still no answers to their formation rate or age. In addition to the hydrochemical arguments presented earlier, we now present further steps to obtain quantitative estimates of dissolution rate.

To detect active dissolution and precipitation on a short temporal scale, Johnston et al. [61] used specially designed, finely polished limestone tablets left under exposure in Pisani Passage in either cup water or under active drip spot for various periods of time. The changes on the surface of the tablets were observed by scanning electron microscope (SEM), while the precipitation or dissolution rates were obtained by stereoscopic imaging and 3D analysis. For example, the tablet immersed in RD5a cup (cup adjacent to RD5) showed pronounced surface etching under exposure for 28 weeks (7 months), which included the summer period of 2018 (Mar–Oct). The dissolution rate was calculated to be 0.01–0.025 mm/yr or an average of –0.014 mm/yr, which was the first estimate for dissolution rate in corrosion cups to date. At the control sites in the Red Hall (RD Pool and RD4), a seasonal fluctuation between precipitation and dissolution was observed due to both etched surfaces and calcite crystals grown on the surface. These tablets showed dissolution in summer and precipitation in winter, totalling 0.0115 mm/yr of precipitation [61].

Another approach to calculating dissolution rate and more generally the dissolution dynamics in cups has been to use a mass balance based on the available time series data (SEC and drip count). The main premise is that the difference in Ca concentration between drip c^{drip} and the cup c^{cup} (as shown in section 4.2.3.) corresponds to the amount of Ca that must have precipitated or dissolved in the cup. We assume ideal mixing between cup water and dripwater and instantaneous reactions. The amount of calcite removed from the cup is proportional to the change of Ca concentration in the cup and the amount of water leaving the cup. Therefore, the drainage rate of the water from the cup Q_{out} must be estimated or calculated. Finally, the amount of calcite m_{cc} precipitated or dissolved in a given period of time is equal in mg:

$$m_{cc} = (c^{cup} - c^{drip})Q_{out}Mt, \tag{4}$$

where Ca concentrations are in mmol/L, Q_{out} is in mL/min, M is the molar mass of calcite (100.09 g/mol) and t is the time interval in minutes. We used the data from the RD7 cup and drip, which have the longest time series of the SEC and the drip discharge (about 6 months, 8/06/2020–30/12/2020, with a resolution of 10 minutes), but not without interruptions. Unfortunately, the drainage rate for this cup could not be determined experimentally, so another cup was chosen. Since the substitute cup is about 11 times smaller than the RD7 cup, we recognise that the difference in shape, size and rock medium surely introduces uncertainty into our calculation procedure.

The following calculations are necessary to obtain the parameters for Eq. 4:

1) The time series of the Ca concentration in the cup c^{cup} results from a strong linear relationship with SEC of the manually measured drips and cups (equation in Figure 10c).
2) The time series c^{drip} was calculated from a strong linear relationship between c^{cup} and c^{drip} for RD7 cup/drip samples ($n = 5$; $\rho = 0.9960$, $R^2 = 0.9894$; $c^{drip} = 0.77c^{cup} + 0.34$).
3) The drip discharge Q_{drip} was calculated from the continuous recording of drip count N, as described in the section 2.3. of Materials and Methods.
4) The calculation of the drainage rate Q_{out} required an on-site experiment. A selected cup near RD5 with a diameter of 3 cm and a depth of 8 cm was filled with water and connected to a graduated cylinder via siphon. Both the cup and the cylinder were covered to limit the water inflow. The natural drainage of water from the cup was followed by time-lapse photography of the graduated cylinder at 30-minute intervals over a period of 40 hours. The volume change in the cylinder and in the cup is equal to the amount of water drained from the cup, $\Delta V_{tot} = Q_{out}\Delta t$. This gives the relationship between the

drainage rate and the water level h_w in the cup. We converted this value to cup water volume V and normalised it based on the maximum water content in the cup V_{max}, so that Q_{out} is a function of cup water content $\frac{V}{V_{max}}$. The data points were fitted to an exponential curve $Q_{out} = Q_{min} + Ae^{-\frac{V}{V_{max}}\tau}$ ($n = 39$; $R^2 = 0.8893$), where the fitting parameters were Q_{min} (the minimum discharge; 0.05 mL/min), A, the amplitude (0.0012), and τ, the decay constant (–0.13). The V_{max} of the cup was measured to be ~57 mL.

The calcite precipitation/dissolution m_{cc} in the cup is then calculated step by step using the calculated time series:

1) First, the empty cup is filled with $V = Q_{drip}t$ of water.
2) Q_{out} is calculated based on the current and maximum water content of the cup V and V_{max} respectively.
3) The corrected water volume in the cup is calculated as $V - Q_{out}t$.
4) The current cup water volume is now the sum of the previously corrected volume and the volume of the newly arrived drip water ($Q_{drip}t$).
5) With the values of c^{cup}, c^{drip} and Q_{out} for each successive step, m_{cc} is calculated according to Eq. 4.

Steps 2–5 are then repeated until the end of the available time series. Each time the cup is filled beyond the V_{max} volume, the maximum Q_{out} is reached (2.68 mL/min) and the water volume does not decrease again until $Q_{drip} < Q_{out}$. Similarly, the minimum Q_{out} (0.05 mL/min) exceeds the minimum Q_{drip} (0.014 mL/min, ~1 drop in 5 min) and therefore the cup can run dry during occasional dry periods. Figure 15a shows the results of the previous calculations, while Figure 15b compares the water dynamics in the cup with the $p\text{CO}_2$ in the cave air, the Ca concentrations and the change in the mass of precipitated (positive) or dissolved (negative) calcite m_{cc}. The dissolution dynamics as shown by the m_{cc} are consistent with the control mechanisms described in the previous section. The strongest dissolution is expected under high CO_2 conditions, when the difference between the calcium concentration in the cup water and in the dripwater is greatest, and when the dripping is enhanced, resulting in the highest drainage rate.

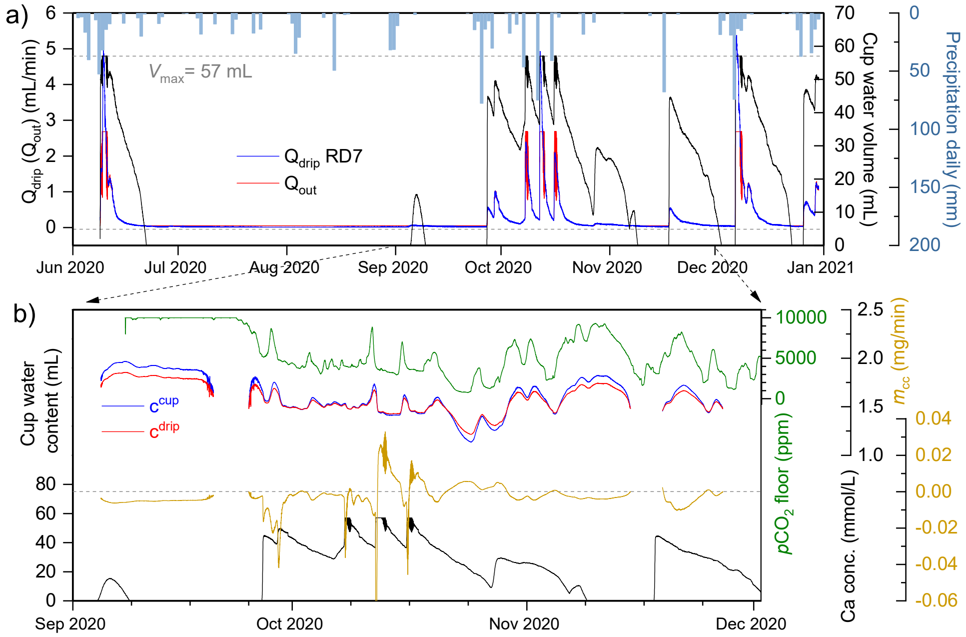

Figure 15. (**a**) Results of the calculation of the dynamics of the cup water volume from the dripwater discharge Q_{drip} (blue curve) and the drainage rate Q_{out} (red curve) compared to the daily precipitation (blue bars). The maximum volume V_{max} was calculated to be 57 mL, while the minimum

volume can drop to zero (dry cup). (**b**) Comparison between pCO_2 at the floor level, the Ca concentration in cup and in the drip, the change in calcite mass (precipitation – positive; dissolution – negative) and cup water content. The largest negative spikes in m_{cc} occur when pCO_2 is high, just before the cup is full and when Q_{out} is highest.

From the total cumulative change in m_{cc} over 1993 hours (~83 days, ~12 weeks), we get a net change of –33 mg or 12 mm^3 calcite. To convert this value into a precipitation or dissolution rate (in mm/yr), we would need a growth model for a cup. Since we do not yet have such a model, we make a rough estimate by dividing the volume of calcite removed by an average wetted surface area in the cup. From the volume-height relation and the radius of the cup (assuming a cylinder with a radius of 1.5 cm and a depth of 8 cm) we get the average wetted surface S_w = 8.5 cm^2. Dividing the volume of removed calcite with the wetted surface gives a dissolution rate of –0.014 mm. While this value is consistent with the estimate obtained from the limestone tablet, the time period of this estimate (Sept–Nov) is ~2.3 times shorter and excludes the summer period, so the dissolution rate estimate could be a few times higher or even similar if the winter period precipitation were included. Nevertheless, if go further and speculate on the age of the corrosion cups and also assume that the obtained dissolution rate corresponds to the annual estimate, i.e. –0.014 mm/yr, is only vertical and constant in time, then the 8 cm deep cup would form in ~6000 years.

Although the results remain highly speculative and uncertain due to the combination of various correlations and assumptions, and the neglect of the kinetics of carbonate chemistry or other variables, the calculation nevertheless provides a reasonable value. Although our primary intention was to provide a qualitative measure, we have nevertheless proposed a method for estimating the dissolution rate that could certainly be further developed and refined. The model of the evolution of the corrosion cup shape could also be developed with more complex modelling and with additional measurements in the cave.

5. Conclusions

In the Pisani Passage of Postojna Cave, Slovenia, several hundred cup-shaped corrosion features and stalagmites affected by severe dissolution were found. In this work we investigated the most likely variables affecting the formation of corrosion cups: host rock composition, hydrology, spatial and temporal distribution of pCO_2 in cave air, and geochemical evolution of water from the vadose zone, as cave dripwater and within the corrosion cups. We found that the thickness of the vadose zone determines the initial calcium concentration of the dripwater, which decreases from the entrance of Pisani Passage (~100 m overburden and ~2 mmol/L Ca) towards Red Hall at the end of Pisani Passage (~30 m overburden and ~1.5 mmol/L Ca), where most dissolution features were found. Seasonal cave ventilation controls the temporal dynamics of pCO_2, with minima in winter and maxima in summer, and the same variation imprints variation in dripwater geochemistry, with positive saturation indices in winter and negative in summer. The configuration of the airflow pathways favours the accumulation of CO_2 in the Red Hall and especially near the floor, where the cups are located. Such a microclimatic setting allows the dripwater, which is low in calcium, to shift towards undersaturation, leading to dissolution of the rock and speleothems. Conversely, at the control drip sites, precipitation is favoured by the overall higher Ca concentration and lower average pCO_2 of the cave air. We also found signs that the proportion between precipitation and dissolution changes over time, illustrated by corrosion cups now covered by flowstone. The results of this study shed new light on fundamental karst processes and effects on the speleothem incubator, the understanding of which is crucial for palaeoclimate research.

Author Contributions: Conceptualisation, L.K., F.G. and V.E.J.; methodology, L.K., F.G. and V.E.J.; investigation, L.K., F.G. and V.E.J.; data curation, L.K.; writing—original draft preparation, L.K.;

writing—review and editing, L.K., F.G. and V.E.J.; visualisation, L.K. All authors have read and agreed to the published version of the manuscript.

Funding: The research was partly funded by the project "Methodology for monitoring the sustainable use of karst show caves with automatic measurements – role model – Postojna cave" (L6-9397), which was financially supported by the Slovenian Research Agency. LK's work was supported by the Young Researchers Programme of the Slovenian Research Agency.

Acknowledgements: We thank Boštjan Grašič and Primož Mlakar for setting up and maintaining the monitoring system in Postojna Cave. The automatic titrator and ion chromatograph of the laboratory of the Karst Research Institute ZRC SAZU was funded by the project "DEVELOPMENT OF RESEARCH INFRASTRUCTURE FOR THE INTERNATIONAL COMPETITIVENESS OF THE SLOVENIAN RRI SPACE – RI-SI-LifeWatch". The operation is co-financed by the Republic of Slovenia, Ministry of Education and Sport and the European Union from the European Regional Development Fund. We thank Dr. Jan Rohovec from the Institute of Geology of the Czech Academy of Sciences for the sample preparation and elemental analyses of the corrosion cups.

List of Abbreviations:

A	amplitude in calculation of drainage rate
c^{cup}	Ca concentration in cup water
c^{drip}	Ca concentration in dripwater
h_w	water level in the cup
log(pCO$_2$)	logarithm with base ten of CO$_2$ partial pressure
m_0 and S	fitting parameters in the calculation of drip discharge
m_{cc}	dissolution or precipitation rate of calcite
N	drip count
pCO$_2$	partial pressure of CO$_2$ gas in air
pCO$_{2(eq)}$	partial pressure of CO$_2$ gas in equilibrium with solution
pCO$_{2(sat)}$	partial pressure of CO$_2$ gas in equilibrium with solution and saturated in respect to calcite
PCP	prior calcite precipitation
PP	Pisani Passage
Q_{drip}	drip discharge
Q_{min}	minimal cup drainage rate
Q_{out}	cup drainage rate
R^2	coefficient of determination
RD	Red Hall
SEC	specific electroconductivity (compensated at 25°C)
SEM	scanning electron microscope
SI$_{cc}$	calcite saturation index
S_w	wetted cup wall surface
T	water temperature
t	time period
V	the water volume in a cup
V_{max}	maximum cup water content
WH	White Hall
Δt	time interval
ΔV_{tot}	the total volume change in the cylinder-cup experiment
ρ	Pearson's correlation factor
ρ_w	water density
τ	decay constant in calculation of drainage rate

References

1. Fairchild, I.J.; Baker, A. *Speleothem Science: From Process to Past Environments*; A John Wiley & Sons, Ltd., 2012; ISBN 9781405196208.
2. Lachniet, M.S. Climatic and Environmental Controls on Speleothem Oxygen-Isotope Values. *Quat. Sci. Rev.* **2009**, *28*, 412–432, doi:10.1016/j.quascirev.2008.10.021.
3. Spötl, C.; Fairchild, I.J.; Tooth, A.F. Cave Air Control on Dripwater Geochemistry, Obir Caves (Austria): Implications for Speleothem Deposition in Dynamically Ventilated Caves. *Geochim. Cosmochim. Acta* **2005**, *69*, 2451–2468, doi:10.1016/j.gca.2004.12.009.
4. Baldini, J.U.L.; Lechleitner, F.A.; Breitenbach, S.F.M.; van Hunen, J.; Baldini, L.M.; Wynn, P.M.; Jamieson, R.A.; Ridley, H.E.; Baker, A.J.; Walczak, I.W.; et al. Detecting and Quantifying Palaeoseasonality in Stalagmites Using Geochemical and Modelling Approaches. *Quat. Sci. Rev.* **2021**, *254*, 106784, doi:10.1016/j.quascirev.2020.106784.
5. Sherwin, C.M.; Baldini, J.U.L. Cave Air and Hydrological Controls on Prior Calcite Precipitation and Stalagmite Growth Rates: Implications for Palaeoclimate Reconstructions Using Speleothems. *Geochim. Cosmochim. Acta* **2011**, *75*, 3915–3929, doi:10.1016/j.gca.2011.04.020.
6. Hartmann, A.; Baker, A. Modelling Karst Vadose Zone Hydrology and Its Relevance for Paleoclimate Reconstruction. *Earth-Science Rev.* **2017**, *172*, 178–192, doi:10.1016/j.earscirev.2017.08.001.
7. Surić, M.; Czuppon, G.; Lončarić, R.; Bočić, N.; Lončar, N.; Bajo, P.; Drysdale, R.N. Stable Isotope Hydrology of Cave Groundwater and Its Relevance for Speleothem-Based Paleoenvironmental Reconstruction in Croatia. *Water (Switzerland)* **2020**, *12*, doi:10.3390/W12092386.
8. Mattey, D.P.; Atkinson, T.C.; Barker, J.A.; Fisher, R.; Latin, J.P.; Durrell, R.; Ainsworth, M. Carbon Dioxide, Ground Air and Carbon Cycling in Gibraltar Karst. *Geochim. Cosmochim. Acta* **2016**, *184*, 88–113, doi:10.1016/j.gca.2016.01.041.
9. Baldini, J.U.L.; Baldini, L.M.; McDermott, F.; Clipson, N. Carbon Dioxide Sources, Sinks, and Spatial Variability in Shallow Temperate Zone Caves: Evidence from Ballynamintra Cave, Ireland. *J. Cave Karst Stud.* **2006**, *68*, 4–11.
10. Breecker, D.O.; Payne, A.E.; Quade, J.; Banner, J.L.; Ball, C.E.; Meyer, K.W.; Cowan, B.D. The Sources and Sinks of CO2 in Caves under Mixed Woodland and Grassland Vegetation. *Geochim. Cosmochim. Acta* **2012**, *96*, 230–246, doi:10.1016/j.gca.2012.08.023.
11. Milanolo, S.; Gabrovšek, F. Analysis of Carbon Dioxide Variations in the Atmosphere of Srednja Bijambarska Cave, Bosnia and Herzegovina. *Boundary-Layer Meteorol* **2009**, *131*, 479–493, doi:10.1007/s10546-009-9375-5.
12. Banner, J.L.; Guilfoyle, A.; James, E.W.; Stern, L.A.; Musgrove, M. Seasonal Variations in Modern Speleothem Calcite Growth in Central Texas, U.S.A. *J. Sediment. Res.* **2007**, *77*, 615–622, doi:10.2110/jsr.2007.065.
13. Baldini, J.U.L.; McDermott, F.; Hoffmann, D.L.; Richards, D.A.; Clipson, N. Very High-Frequency and Seasonal Cave Atmosphere PCO2 Variability: Implications for Stalagmite Growth and Oxygen Isotope-Based Paleoclimate Records. *Earth Planet. Sci. Lett.* **2008**, *272*, 118–129, doi:https://doi.org/10.1016/j.epsl.2008.04.031.
14. Baldini, J.U.L. Cave Atmosphere Controls on Stalagmite Growth Rate and Palaeoclimate Records. *Geol. Soc. Spec. Publ.* **2010**, *336*, 283–294, doi:10.1144/SP336.15.
15. Kukuljan, L.; Gabrovšek, F.; Covington, M.D.; Johnston, V.E. CO2 Dynamics and Heterogeneity in a Cave Atmosphere: Role of Ventilation Patterns and Airflow Pathways. *Theor. Appl. Climatol.* **2021**, doi:10.1007/s00704-021-03722-w.
16. Whitaker, T.; Jones, D.; Baldini, J.U.L.; Baker, A.J. A High-Resolution Spatial Survey of Cave Air Carbon Dioxide Concentrations in Scoska Cave (North Yorkshire, UK): Implications for Calcite Deposition and Re-Dissolution. *Cave Karst Sci.* **2009**, *36*, 85–92.
17. Noronha, A.L.; Hardt, B.F.; Banner, J.L.; Jenson, J.W.; Partin, J.W.; James, E.W.; Lander, M.A.; Bautista, K.K. Trade Winds Drive Pronounced Seasonality in Carbonate Chemistry in a Tropical Western Pacific Island Cave—Implications for

Speleothem Paleoclimatology. *Geochemistry, Geophys. Geosystems* **2017**, *18*, 384–399, doi:10.1002/2016GC006644.

18. Frisia, S.; Fairchild, I.; Fohlmeister, J.; Miorandi, R.; Spötl, C.; Borsato, A. *Carbon Mass-Balance Modelling and Carbon Isotope Exchange Processes in Dynamic Caves*; 2011; Vol. 75;.
19. James, E.W.; Banner, J.L.; Hardt, B. A Global Model for Cave Ventilation and Seasonal Bias in Speleothem Paleoclimate Records. *Geochemistry, Geophys. Geosystems* **2015**, *16*, 1044–1051, doi:10.1002/2014GC005658.
20. Borsato, A.; Johnston, V.E.; Frisia, S.; Miorandi, R.; Corradini, F. Temperature and Altitudinal Influence on Karst Dripwater Chemistry: Implications for Regional-Scale Palaeoclimate Reconstructions from Speleothems. *Geochim. Cosmochim. Acta* **2016**, *177*, 275–297, doi:10.1016/j.gca.2015.11.043.
21. Railsback, L.B.; Liang, F.; Vidal Romaní, J.R.; Grandal-d'Anglade, A.; Vaqueiro Rodríguez, M.; Santos Fidalgo, L.; Fernández Mosquera, D.; Cheng, H.; Edwards, R.L. Petrographic and Isotopic Evidence for Holocene Long-Term Climate Change and Shorter-Term Environmental Shifts from a Stalagmite from the Serra Do Courel of Northwestern Spain, and Implications for Climatic History across Europe and the Mediterranean. *Palaeogeogr. Palaeoclimatol. Palaeoecol.* **2011**, *305*, 172–184, doi:10.1016/j.palaeo.2011.02.030.
22. Banner, J.L.; Guilfoyle, A.; James, E.W.; Stern, L.A.; Musgrove, M. Seasonal Variations in Modern Speleothem Calcite Growth in Central Texas, U.S.A. *J. Sediment. Res.* **2007**, *77*, 615–622, doi:10.2110/jsr.2007.065.
23. Baldini, J.U.L.; McDermott, F.; Fairchild, I.J. Spatial Variability in Cave Drip Water Hydrochemistry: Implications for Stalagmite Paleoclimate Records. *Chem. Geol.* **2006**, *235*, 390–404, doi:10.1016/j.chemgeo.2006.08.005.
24. White, J.H.; Domínguez-Villar, D.; Hartland, A. Condensation Corrosion Alters the Oxygen and Carbon Isotope Ratios of Speleothem and Limestone Surfaces. *Results in Geochemistry* **2021**, *2*, 100008, doi:10.1016/j.ringeo.2021.100008.
25. White, W.B. Chemistry and Karst. *Acta Carsologica* **2015**, *44*, 349–362.
26. Johnston, V.; Martín-Pérez, A.; Skok, S.; Mulec, J. Microbially-Mediated Carbonate Dissolution and Precipitation; towards a Protocol for Ex-Situ, Cave-Analogue Cultivation Experiments. *Int. J. Speleol.* **2021**, *50*, 137–155, doi:10.5038/1827-806x.50.2.2372.
27. Spötl, C.; Pavuza, R.; Dublyansky, Y. Hypogene Caves in Austria. *Hypogene Speleogenes. Karst Hydrogeol. Artesian Basins. Spec. Pap. 1* **2009**, 121–127.
28. Treble, P.C.; Fairchild, I.J.; Griffiths, A.; Baker, A.; Meredith, K.T.; Wood, A.; McGuire, E. Impacts of Cave Air Ventilation and In-Cave Prior Calcite Precipitation on Golgotha Cave Dripwater Chemistry, Southwest Australia. *Quat. Sci. Rev.* **2015**, *127*, 61–72, doi:10.1016/j.quascirev.2015.06.001.
29. Faimon, J..; Ličbinská, M.. b; Zajíček, P..; Sracek, O.. e Partial Pressures of CO2 in Epikarstic Zone Deduced from Hydrogeochemistry of Permanent Drips, the Moravian Karst, Czech Republic [Delni Tlak CO2 V Epikraški Coni, Kot Ga Razkrivajo Hidrokemične Raziskave Stalnih Vodnih Curkov]. *Acta Carsologica* **2012**, *41*, 47–57.
30. Milanolo, S.; Gabrovšek, F. Estimation of Carbon Dioxide Flux Degassing from Percolating Waters in a Karst Cave: Case Study from Bijambare Cave, Bosnia and Herzegovina. *Chemie der Erde* **2015**, *75*, 465–474, doi:10.1016/j.chemer.2015.10.004.
31. Hansen, M.; Dreybrodt, W.; Scholz, D. Chemical Evolution of Dissolved Inorganic Carbon Species Flowing in Thin Water Films and Its Implications for (Rapid) Degassing of CO2 during Speleothem Growth. *Geochim. Cosmochim. Acta* **2013**, *107*, 242–251, doi:10.1016/j.gca.2013.01.006.
32. Prelovšek, M.; Šebela, S.; Turk, J. Carbon Dioxide in Postojna Cave (Slovenia): Spatial Distribution, Seasonal Dynamics and Evaluation of Plausible Sources and Sinks. *Environ. Earth Sci.* **2018**, *77*, doi:10.1007/s12665-018-7459-6.
33. Gregorič, A.; Vaupotič, J.; Gabrovšek, F. Reasons for Large Fluctuation of Radon and CO2 Levels in a Dead-End Passage of a Karst Cave (Postojna Cave, Slovenia). *Nat. Hazards Earth Syst. Sci.* **2013**, *13*, 287–297, doi:10.5194/nhess-13-287-2013.
34. Šebela, S. Postojna—Planina Cave System, Slovenia. In *Encyclopedia of caves*; White, W.B., Culver, D.C., Pipan, T.B.T.-E. of C. (Third E., Eds.; Academic Press, 2019; pp. 812–821 ISBN 978-0-12-814124-3.

35. Šebela, S. Accesses from the Surface to the Postojna Cave System. *Ann. Ser. Hist. Nat.* **2010**, *20*, 55–64.
36. Šebela, S.; Vaupotič, J.; Košťák, B.; Stemberk, J. Direct Measurement of Present-Day Tectonic Movement and Associated Radon Flux in Postojna Cave, Slovenia. *J. Cave Karst Stud.* **2010**, *72*, 21–34, doi:10.4311/jcks2009es0077.
37. ARSO Ministry of the Environment and Spatial Planning, Slovenian Environmental Agency Available online: http://meteo.arso.gov.si/met/en/ (accessed on 6 May 2021).
38. Šebela, S. Geological Characteristics of Pisani Rov in Postojna Cave [in Slovene]. *Acta Carsologica* **1992**, *XXI*, 97–116.
39. Šebela, S. Broken Speleothems as Indicators of Tectonic Movements. *Acta Carsologica* **2008**, *37*, 51–62, doi:10.3986/ac.v37i1.159.
40. Krajnc, B.; Ferlan, M.; Ogrinc, N. Soil CO2 Sources above a Subterranean Cave—Pisani Rov (Postojna Cave, Slovenia). *J. Soils Sediments* **2017**, *17*, 1883–1892, doi:10.1007/s11368-016-1543-x.
41. Kogovšek, J. Water Percolation and Sinter Deposition in Pisani Rov of Postojnska Jama [in Slovene]. *Acta Carsologica* **1983**, *11*, 59–76.
42. Mattey, D.P.; Collister, C. Acoustic Drip Counters for Environmental Monitoring. *BCRA Cave Radio Electron. Gr.* **2008**, *70*, 14–17.
43. Collister, C.; Mattey, D. Controls on Water Drop Volume at Speleothem Drip Sites: An Experimental Study. *J. Hydrol.* **2008**, *358*, 259–267, doi:10.1016/j.jhydrol.2008.06.008.
44. Appelo, T.; Postma, D. *Geochemistry, Groundwater and Pollution (Second Edition)*; 2005;
45. Kogovšek, J. Distribution of Some Elements during Sinter Forming in the Karst Caves [in Slovene]. *Acta Carsologica* **1981**, *9*, 114–126.
46. Baker, A.; Barnes, W.L.; Smart, P.L. Variations in the Discharge and Organic Matter Content of Stalagmite Drip Waters in Lower Cave, Bristol. *Hydrol. Process.* **1997**, *11*, 1541–1555, doi:10.1002/(SICI)1099-1085(199709)11:11<1541::AID-HYP484>3.0.CO;2-Z.
47. Kogovšek, J.; Petrič, M. Solute Transport Processes in a Karst Vadose Zone Characterized by Long-Term Tracer Tests (the Cave System of Postojnska Jama, Slovenia). *J. Hydrol.* **2014**, *519*, 1205–1213, doi:10.1016/j.jhydrol.2014.08.047.
48. Kukuljan, L.; Gabrovsek, F.; Covington, M. The Relative Importance of Wind-Driven and Chimney Effect Cave Ventilation: Observations in Postojna Cave (Slovenia). *Int. J. Speleol.* **2021**, *50*, 275–288, doi:10.5038/1827-806x.50.3.2392.
49. Krawczyk, W.E.; Ford, D.C. Correlating Specific Conductivity with Total Hardness in Limestone and Dolomite Karst Waters. *Earth Surf. Process. Landforms* **2006**, *31*, 221–234, doi:10.1002/esp.1232.
50. Vokal, B.; Obeli, B.; Genty, D.; Kobal, I.; Obeliê, B. Chemistry Measurements of Dripping Water in Postojna Cave. *Acta Carsologica* **1999**.
51. Šebela, S.; Čar, J. Velika Jeršanova Doline - A Former Collapse Doline. *Acta Carsologica* **2000**, 201-212(12).
52. Gams, I. Factors and Dynamics of Corrosion of the Carbonatic Rocks in the Dinaric and Alpine Karst of Slovenia (Yugoslavia) [in Slovene]. *Geogr. Vestn.* **1966**, *XXXVIII*, 11–68.
53. Baker, A.; Flemons, I.; Andersen, M.S.; Coleborn, K.; Treble, P.C. What Determines the Calcium Concentration of Speleothem-Forming Drip Waters? *Glob. Planet. Change* **2016**, *143*, 152–161, doi:10.1016/j.gloplacha.2016.06.001.
54. Noronha, A.L.; Johnson, K.R.; Southon, J.R.; Hu, C.; Ruan, J.; McCabe-Glynn, S. Radiocarbon Evidence for Decomposition of Aged Organic Matter in the Vadose Zone as the Main Source of Speleothem Carbon. *Quat. Sci. Rev.* **2015**, *127*, 37–47, doi:10.1016/j.quascirev.2015.05.021.
55. Bergel, S.J.; Carlson, P.E.; Larson, T.E.; Wood, C.T.; Johnson, K.R.; Banner, J.L.; Breecker, D.O. Constraining the Subsoil Carbon Source to Cave-Air CO2 and Speleothem Calcite in Central Texas. *Geochim. Cosmochim. Acta* **2017**, *217*, 112–127, doi:10.1016/j.gca.2017.08.017.
56. Blecha, M.; Faimon, J. Karst Soils: Dependence of CO2 Concentrations on Pore Dimension. *Acta Carsologica* **2014**, *43*, 55–64.
57. Treble, P.C.; Fairchild, I.J.; Baker, A.; Meredith, K.T.; Andersen, M.S.; Salmon, S.U.; Bradley, C.; Wynn, P.M.; Hankin, S.I.;

Wood, A.; et al. Roles of Forest Bioproductivity, Transpiration and Fire in a Nine-Year Record of Cave Dripwater Chemistry from Southwest Australia. *Geochim. Cosmochim. Acta* **2016**, *184*, 132–150, doi:10.1016/j.gca.2016.04.017.

58. Pracný, P.; Faimon, J.; Sracek, O.; Kabelka, L.; Hebelka, J. Anomalous Drip in the Punkva Caves (Moravian Karst): Relevant Implications for Paleoclimatic Proxies. *Hydrol. Process.* **2016**, *30*, 1506–1520, doi:10.1002/hyp.10731.
59. Pracný, P.; Faimon, J.; Kabelka, L.; Hebelka, J. Variations of Carbon Dioxide in the Air and Dripwaters of Punkva Caves (Moravian Karst, Czech Republic). *Carbonates and Evaporites* **2016**, *31*, 375–386, doi:10.1007/s13146-015-0259-0.
60. Smith, A.C.; Wynn, P.M.; Barker, P.A.; Leng, M.J. Drip Water Electrical Conductivity as an Indicator of Cave Ventilation at the Event Scale. *Sci. Total Environ.* **2015**, *532*, 517–527, doi:10.1016/j.scitotenv.2015.06.037.
61. Johnston, V.E.; Košir, A.; Martín-Pérez, A. *Evaluating Carbonate Dissolution and Precipitation in a Short Time-Frame Using SEM: Techniques and Preliminary Results from Postojna Cave, Slovenia*;